Optical and Quantum Electronics (2023) 55:1081
https://doi.org/10.1007/s11082-023-05383-7

Performance of density functional theory for calculating the electronic, static, and dynamic nonlinear optical properties of asymmetric (3*E*,5*E*)-3,5-dibenzylidene-piperidin-4-one derivatives

Lala Adetia Marlina[1] · Aulia Sukma Hutama[2] · Septiana Nur Zanah[2] · Mokhammad Fajar Pradipta[2] · Wilin Julian Sari[1] · Wahyu Dita Saputri[1]

Received: 31 July 2023 / Accepted: 4 September 2023 / Published online: 26 September 2023

Abstract
The electronic charge delocalization in organic compounds with a donor–acceptor system allows them to exhibit excellent nonlinear optical characteristics. From the perspective of conjugation, mono-carbonyl curcuminoids also have a fascinating skeleton. Interesting chemical structures of the (3*E*,5*E*)-3,5-dibenzylidene-piperidin-4-one derivatives motivate us to perform density functional theory-based studies. In investigating the derivates, geometric parameters, highest occupied molecular orbital (HOMO)–lowest unoccupied molecular orbital (LUMO) energies, and nonlinear optical (NLO) parameters calculations were performed using B3LYP/6-311++G(*d*,*p*) level of theory. Root mean square error (RMSE) calculations revealed excellent agreement between calculated and experimental parameters. The molecular stability of chalcone derivatives was investigated using molecular electrostatic potential analyses, which were also used to gain information regarding atomic charges. Calculated HOMO–LUMO energies showed that charge transfer interactions occur within the molecules. The HOMO and LUMO energies were used to compute hardness, softness, ionization potential, and electrophilicity. The λ_{max} values of the investigated compounds are greater than that of the reference compound. Among all other derivatives, **B4** has the highest amplitude of static linear polarizability (α_{tot}) and first total hyperpolarizability (β_{tot}) values at 101.15 and 554.11×10^{-30} esu, respectively. Compelling NLO findings reveal that bis-chalcones-based derivatives could substantially contribute to NLO technology.

Keywords (3*E*,5*E*)-3,5-dibenzylidene-piperidin-4-one · Nonlinear optic · Quantum chemical study · Density functional theory

1 Introduction

The discovery of laser has accelerated research into nonlinear optical (NLO) response of materials under intense optical fields, which comes from second-order phenomena involving frequency conversion (Fejer 1994; Lifshitz et al. 2005) and third-order phenomena of

Extended author information available on the last page of the article

nonlinear refraction (NLR) and nonlinear absorption (NLA) (Christodoulides et al. 2010). The structural symmetry constraint restricts the crystals' availability to those with second-order NLO interactions. This constraint involves extensive research into the third-order NLO, which is the lowest-order non-linear response in the centrosymmetric medium and is used in a variety of applications such as signal processing (Garmire 2013), spectroscopy (Ito and Mikami 1980) and microfabrication (Kuebler and Rumi 2005).

Organic molecules are preferred for NLO tools in electronics and semiconductor devices due to their ease of availability, low cost, and remarkable NLO responsiveness (Bosshard et al. 2001; Ivanova and Spiteller 2010; Zyss 2013). Some organic molecule structures allow an intense charge transfer state from the electron donor (D) to the electron acceptor (A) moiety to increase the NLO response in the donor–acceptor structure. This configuration strengthens the polarization capabilities and optical gaps of the NLO compounds (Sutradhar and Misra 2021). By altering the configuration of the suitable donor and acceptor substituent on the D–π–A framework, where –π– stands for a π bridge, the π-conjugated systems can manipulate intramolecular charge transfer (ICT) and NLO properties (Hrobarik et al. 2010). Additionally, some researchers found that by increasing π-electron delocalization, zwitterionic D and A groups positioned at the opposing ends of conjugated chromophores can enhance their NLO response, making the substance appropriate for optoelectronic material (Majumder and Misra 2018). Thus, it is crucial for structural modification of electron donors and electron acceptors in designing D–π–A systems (Ammasi et al. 2023a; Ponnusamy Munusamy et al. 2022) as a practical approach to obtaining high-performance NLO materials.

It has also been shown that the first-order optical nonlinearities grow with a push–pull effect from D/A substituents (Ammasi et al. 2023b), relative position (Gandhimathi et al. 2013), conjugation length (Erickson et al. 2016), intermolecular interactions (Yoneda et al. 2014), and geometrical symmetric effects (Muhammad 2022). The interaction effectiveness between the D and A parts determines the degree to which charge is transferred between the molecules, improving the NLO responses. Different D and A substituents are used to design asymmetric and symmetric molecules that optimize and enhance NLO properties (Cai et al. 2017).

Among general organic NLO materials, organic chalcone NLO derivatives have intrigued scientists and researchers worldwide due to their numerous uses in medical and NLO technical fields (Feng et al. 2014; Matos et al. 2015; Tejkiran et al. 2016; Vazquez-Rodriguez et al. 2015; Wei et al. 2016). In addition to the experimental works, several first-principles studies for chalcone, bis-chalcone, and their derivatives have been carried out to investigate their structural, optoelectronic, charge transport, second-order and third-order NLO features (Irfan et al. 2019a, 2019b; Wazzan and Irfan 2019). Considerable work was put into elucidating the structure-property correlations of the molecule to enhance molecular nonlinearities (Virkki et al. 2015; Yushina et al. 2018). Interestingly, due to the asymmetric charge distributions, significant variations have been observed in the signs and magnitudes of NLO polarizabilities (Muhammad et al. 2018; Nakano et al. 2016). Several asymmetry-based substituted materials have been experimentally synthesized and characterized (Muhammad et al. 2018; Nakano et al. 2016). Moreover, the bis-chalcone derivatives with D–π–A structure have a substantially delocalized and asymmetric electron system, resulting in ICT from end to end of the two rings and good NLO characteristics (Muhammad et al. 2017). Incorporating alkyl amine groups at the *para*-position of the chalcone's phenyl ring is another way to improve the donor character and promote charge transfer toward the acceptor (Cigan et al. 2013; Cisse et al. 2011). A comprehensive report on the previous and current progress on strategies to enhance the NLO activity of

materials, particularly bis-chalcone, has been published by one of the authors (see reference (Hutama et al. 2019) for more details).

To attain a comprehensive understanding of the molecular optical nonlinearity from the microscopic regime, theoretical assessments have been considered a critical function compared to the practical output. The theoretical assessments are also used for designing and modifying new or existing chromophores with greater molecular hyperpolarizability by modulating the relevant parameters to yield the optimal desired response (Prasad and Williams 1991). Harnessing the predictive power of computational chemistry offers a unique avenue for unraveling the NLO potential of chalcones in which their properties can then be tailored for specific applications. The selection of the computational method is crucial for precisely determining electronic hyperpolarizabilities. The density functional theory (DFT) approach has been widely utilized to study molecular properties like molecular structure, bond lengths, bond angles, and torsion angles, as well as spectroscopic properties such as ultraviolet–visible (UV–vis), Fourier transform infrared (FTIR), and nuclear magnetic resonance (NMR) spectra (Hussein and Fadhil 2023; Kusumawati et al. 2022; Mary et al. 2015; Panicker et al. 2015; Yousif and Fadhil 2021). This demonstrates that DFT is an effective method for balancing accuracy and computing efficiency.

In the present work, we reported a comparative analysis of the NLO response of asymmetrically end-functionalized (3*E*,5*E*)-3,5-dibenzylidene-1-methylpiperidin-4-one derivatives (Eryanti et al. 2015). We were interested in researching eight chalcone derivatives that principally transfer electrons via the *N*-methyl-4-piperidone bridge. When alkylamine substituents were added to the chalcone's 7-position (i.e., *para*–), push–pull systems with D–π–A structures arose. The primary goal of this study is to conduct a thorough theoretical investigation into the effect of different terminal group substitutions on the optical, NLO, electronic, and charge transfer properties, as well as to provide an in-depth understanding of the relationship between the push–pull effect from D/A substituents and their NLO and electronic properties. Furthermore, numerous molecular-level insights for these novel asymmetric configurations were realized through their frontier molecular orbital (FMO), molecular electrostatic potentials (MEP) maps, and transition density matrix (TDM) plots for a molecular-level understanding of these molecules.

2 Molecular models and computational methodology

This study focuses on the NLO examination of the new bis-chalcone-based compounds. This investigation aims to construct novel chalcone derivatives and investigate their possible NLO characteristics. A D–π–A configuration has been established when a series of bis-chalcone-based derivatives has been developed by modifying alternative donor and acceptor units to a fixed D–π–A architecture (Fig. 1). In the parent molecule, (3*E*,5*E*)-3,5-dibenzylidene-piperidin-4-one, two phenyl rings are connected through the *N*-methyl-4-piperidone bridge. We have adopted the chemical models into two sets, i.e., set **A** and set **B,** depending on the acceptor fragments of the D and A groups in the D–π–A configurations. The donor fragment is dimethylamine fused in each set in one phenyl ring with different acceptor fragments in the other. Both sets consist of four systems, where the *para*-position of other phenyl rings was substituted by sulfonamidyl (system **1**), acetamidyl (system **2**), 2,2,2-trifluoroacetamidyl (system **3**), and 2,2,2-trichloroacetamidyl (system **4**) group. Set **A** and **B** are distinguished by the acceptor fragments in which alkyl amine groups are located at *para*-position, as shown in Fig. 1. The effect of substitution on these

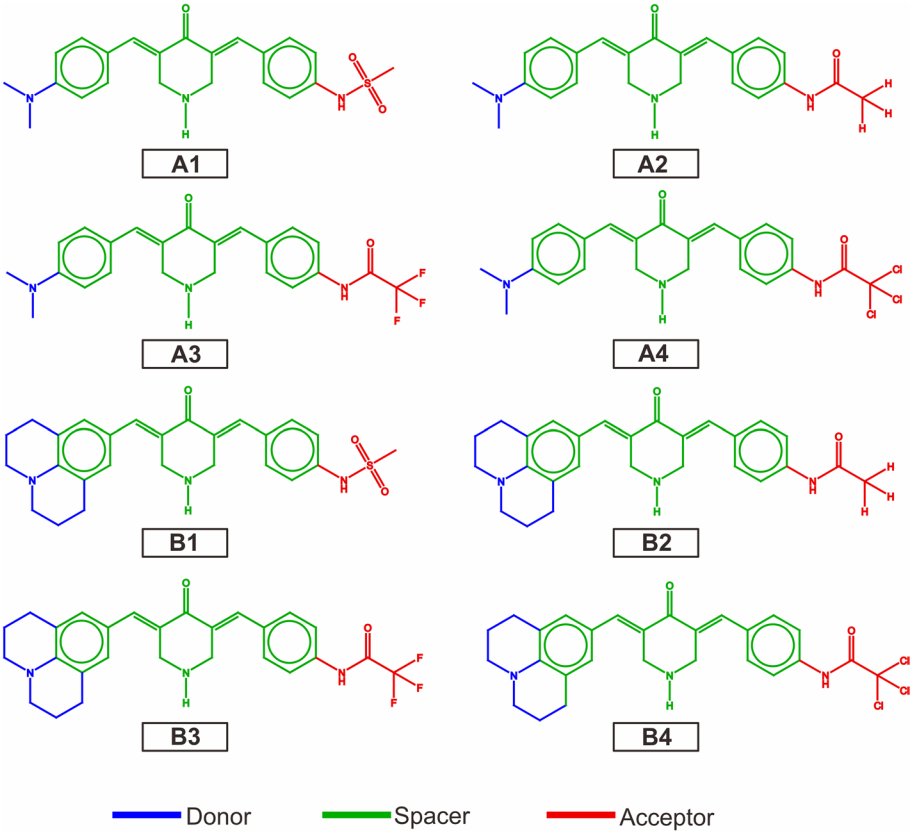

Fig. 1 The molecular structures of the studied organic compounds in the present work

molecules' electronic, optical, and photophysical properties was theoretically explored for the eight derivatives.

DFT and time-dependent (TD)–DFT computations were performed to describe definite guidelines for designing novel NLO compounds and to shed light on how different auxiliary donors, donors and acceptor units affect the ICT, highest occupied molecular orbital (HOMO)—lowest unoccupied molecular orbital (LUMO) energy gap, absorption spectrum, and NLO responses. Gaussian 09 package (Frisch et al. 2013) was used to carry out all the calculations in this study. The optimization of the ground state structures was performed using Becke's three-parameter hybrid function with the Lee–Yang–Parr nonlocal correlation function (B3LYP) (Becke 1993; Lee et al. 1988) in conjunction with a triple-zeta split valence 6-311++G (*d,p*) basis set with the polarization functions for *p* functions added to hydrogen and *d* functions added to the heavy atom (*d,p*). Methanol was employed as the solvent using the implicit solvation conductor polarizable continuum model (CPCM) (Barone and Cossi 1998; Cossi et al. 2003). In addition, for the ground state geometry optimization, we also carried out the calculations using the ωB97XD functional (Chai and Head-Gordon 2008) to assess the reliability of the ground state geometry in comparison with the experimental X-ray crystallography data. The structures obtained via geometry optimization were further used for frequency calculations at the same level of theory to

verify whether the resulting optimized structures are the actual lowest-energy structures and that there is no negative imaginary vibrational frequency. We have employed Multiwfn 3.8 software (Lu and Chen 2012) at B3LYP/6–311 + + G(*d*,*p*) level of theory to plot the TDM map of our designed molecules.

Chemical reactivity descriptors (CRD) parameters, including ionization potential (*IP*) (Maidur et al. 2017), electron affinity (*EA*) (Maidur et al. 2017), chemical potential (μ) (Chattaraj et al. 2003; Hagar et al. 2020; Mary et al. 2015), global hardness (η) (Chidan Kumar et al. 2016), softness (S) (Miar et al. 2021), electronegativity (χ) (Thamarai et al. 2020), and electrophilicity index (ω) (Thamarai et al. 2020) for each conformer were derived from HOMO and LUMO energy as given in Eqs. (1–7) (Mary et al. 2015; Thamarai et al. 2020).

$$IP = -E_{\mathrm{HOMO}} \tag{1}$$

$$EA = -E_{\mathrm{LUMO}} \tag{2}$$

$$\eta = \frac{IP - EA}{2} \tag{3}$$

$$S = \frac{1}{2\eta} \tag{4}$$

$$\chi = \frac{(I + A)}{2} \tag{5}$$

$$\mu = \frac{-(I + A)}{2} \tag{6}$$

$$\omega = \frac{\mu^2}{2\eta} \tag{7}$$

Furthermore, we have evaluated the linear optical properties like excitation energies, maximum absorption wavelength (λ_{max}), oscillator strengths (f_0), and absorption spectra of compounds **A1** to **A4** and **B1** to **B4** at TD-DFT with B3LYP/6-311++G(*d*,*p*) level for the lowest 20 singlet–singlet transitions. The NLO properties were calculated using B3LYP, CAM–B3LYP (Yanai et al. 2004) M06 (Zhao and Truhlar 2008), and ωB97XD DFT functionals with 6-311++G(*d*,*p*) basis set. The various parameters that indicate their applicability as NLO materials are the molecules' electric dipole moment (μ_{tot}), total polarizability (α_{tot}), the magnitude of the first-order hyperpolarizability (β_{tot}), and the vectorial part of the first hyperpolarizability (β_{vec}) (Naik et al. 2020) were estimated using Eqs. (8)–(13).

$$\mu_{tot} = \left(\mu_x^2 + \mu_y^2 + \mu_z^2\right)^{\frac{1}{2}} \tag{8}$$

$$\alpha_{tot} = \frac{1}{3}\left(\alpha_{xx} + \alpha_{yy} + \alpha_{zz}\right) \tag{9}$$

$$\Delta\alpha = \frac{1}{\sqrt{2}}\left[\left(\alpha_{xx}-\alpha_{yy}\right)^2+\left(\alpha_{yy}-\alpha_{zz}\right)^2+\left(\alpha_{zz}-\alpha_{xx}\right)^2+6\alpha_{xz}^2+6\alpha_{xy}^2+6\alpha_{yz}^2\right]^{\frac{1}{2}} \quad (10)$$

$$\beta_{tot} = \left(\beta_x^2+\beta_y^2+\beta_z^2\right)^{1/2} \quad (11)$$

$$\beta_{vec} = \sum_{i=x,y,z}\frac{\mu_i\beta_i}{\mu_{tot}} \quad (12)$$

where $\beta_i (i = x, y, z)$ is given by:

$$\beta_i = (1/3)\sum_{j=x,y,z}\left(\beta_{ijj}+\beta_{jij}+\beta_{jji}\right) \quad (13)$$

The superscripts in Eqs. (8)–(13) indicate their projection to Cartesian axes.

3 Results and discussions

3.1 Validation of method

Due to the advances in computational hardware and software development, the ability to perform computation calculations has substantially improved along with decreased computational costs. However, as the march toward experimental precision continues, the challenge of the method of computation prediction choice persists. To accomplish this purpose, computational approaches are typically compared with experimental data to validate and select a specific method and increase the acceptance of anticipated outcomes based on closeness to the experimental result, which may be required for further properties calculations.

Here, we compared calculated results with existing experimental X-ray crystallography data to validate our approach. However, following previous results of similar research from our group, our current approach has been validated against the experimental data for the title compound (Hutama et al. 2019). Therefore, we further validated the current approach using the methoxy-substituted compound (3*E*,5*E*)-3,5-dibenzylidene-1-methylpiperidin-4-one, where the experimental data for this compound is publicly available (Nesterov 2004). Geometrical properties of the methoxy-substituted (3*E*,5*E*)-3,5-dibenzylidene-1-methylpiperidin-4-one (bond length, bond angle, and dihedral angle) were examined using DFT calculations with B3LYP and ωB97XD methods and 6-311++G(*d*,*p*) basis set. The optimized geometrical parameters and their comparisons to the compound's X-ray crystallography data are given in Table 1. Figure 2 depicts the crystal structure and optimized geometries of the most favorable conformation of the title compound.

As illustrated in Fig. 2a, the molecular structure of the bis-chalcone derivative consists of two styrene rings connected by *α,β*-unsaturated carbonyl, the primary chalcone moiety, which has an *E* configuration. The calculated torsional angle of C8–C7 = C5–C4 is − 178.60° of the compound at B3LYP/6-311++G(*d*,*p*) level of theory. The phenyl ring (C9/C8) makes dihedral angles with molecule planes with a maximum deviation from the plane of 22.22 for O1.

Table 1 Experimental and calculated geometrical parameters for (3*E*,5*E*)-3,5-dibenzylidene-1-methylpiperidin-4-one molecule

Parameter	Experimental	Calculated	
		B3LYP/6–311 + + G(*d*,*p*)	ωB97XD/6–311 + + G(*d*,*p*)
Bond length (Å)			
O1–C4	1.223 (3)	1.226	1.225
O2–C11	1.363 (3)	1.361	1.351
O3–C19	1.363 (4)	1.361	1.352
C3–C15	1.331 (4)	1.351	1.345
C4–C5	1.488 (4)	1.498	1.494
C5–C7	1.351 (4)	1.352	1.345
C7–C8	1.455 (4)	1.459	1.463
C15–C16	1.458 (4)	1.459	1,463
MAD		− 0.0044	− 0.0008
MSE		0.0002	0.0001
RMSE		0.0124	0.0021
MAPE		− 0.3180	− 0.0475
Bond angle (°)			
C11–O2–C14	118.0 (2)	118.78	118.48
C19–O3–C22	118.8 (3)	118.72	118.41
C15–C3–C4	118.1 (3)	116.68	117.13
C15–C3–C2	125.3 (3)	125.09	124.86
C4–C3–C2	116.5 (2)	118.22	117.99
O1–C4–C3	121.5 (3)	121.39	121.43
O1–C4–C5	121.0 (3)	121.38	121.44
C3–C4–C5	117.5 (3)	117.20	117.11
C7–C5–C4	117.1 (3)	116.74	116.95
C7–C5–C6	125.3 (3)	125.04	124.86
C4–C5–C6	117.5 (2)	118.20	118.18
C5–C7–C8	130.8 (3)	130.95	129.77
C3–C15–C16	130.9 (3)	131.04	129.33
MAD		− 0.0869	− 0.2185
MSE		0.0982	0.6204
RMSE		0.3134	0.0971
MAPE		0.0971	0.2185
Dihedral angle (°)			
C4–C5–C7–C8	− 179.5 (3)	− 178.60	− 179.08
C5–C7–C8–C9	− 158.3 (3)	− 158.56	− 153.14
C14–O2–C11–C10	− 175.8 (3)	− 179.60	− 179.98
C4–C3–C15–C16	177.8 (3)	178.74	178.60
C3–C15–C16–C17	154.0 (3)	158.17	151.49
C22–O3–C19–C18	174.0 (3)	179.79	178.71

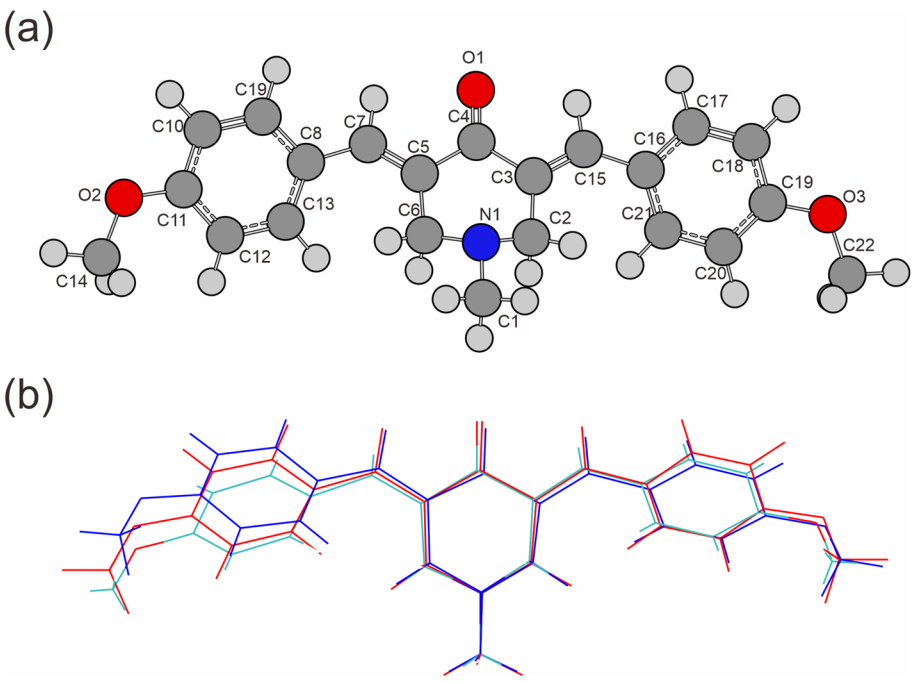

Fig. 2 **a** Optimized geometries of the most favorable conformation of the experimental reference compound of methoxy-substituted (3*E*,5*E*)-3,5-dibenzylidene-1-methylpiperidin-4-one and **b** the superimposition of the experimental (blue), and B3LYP (red) and ωB97XD (green) optimized structure

The estimated C–C bond lengths from the calculated results are slightly longer than the experimental values, as seen in Table 1. The compound's bond lengths align well with the literature's experimental structure (Nesterov 2004). The C5 = C7 and C3 = C15 bond distances of 1.352 Å and 1.351 Å, respectively, are consistent with their double bond character (Bernstein et al. 1995; Ghouili et al. 2014). The C7–C8 bond length of 1.459 Å is intermediate between the double and single bonds. In the molecular structure, the heterocyclic ring adopts a flattened boat conformation; atoms N1 and C4 lie at –0.735 Å and –0.201 Å, respectively, out of the C2/C3/C5/C6 plane (planar within 0.027 Å). The C–C bond lengths of the piperidone moiety ranging from 1.498 Å to 1.509 Å are standard single bonds (Sumithra et al. 2016).

The bond angles of the O1–C4–C5 and C7–C5–C4 molecules are 121.38° and 116.74°, which agree with experimental values. C14–O2–C11–C10, C3–C15–C16–C17 estimated dihedral angles are –179.60° and 158.17°. This region's characteristics were altered because the chalcone moiety was perturbed during the bond's rotation. According to our theoretical analysis, the optimized characteristics have no discernible changes.

The relative analysis revealed that DFT values for bond lengths and angles are higher than X–ray values. However, the opposite occurred in several conditions due to the medium effect since X-ray results referred to the solid state of the molecule, albeit with weak interactions. To further strengthen the correlation between DFT analysis and experimental data, mean absolute deviation (MAD), mean square error (MSE), root

mean square error (RMSE), and mean absolute percentage error (MAPE) can be estimated using Eqs. (14–17).

$$\mathrm{MAD} = \frac{\sum_{t=1}^{n} |EXP - DFT|}{n} \tag{14}$$

$$\mathrm{MSE} = \frac{\sum_{t=1}^{n} (EXP - DFT)^2}{n} \tag{15}$$

$$\mathrm{RMSE} = \sqrt{\frac{\sum_{t=1}^{n} (EXP - DFT)^2}{n}} \tag{16}$$

$$\mathrm{MAPE} = \frac{\sum_{t=1}^{n} \left| \frac{EXP - DFT}{EXP} \right|}{n} \times 100 \tag{17}$$

DFT and EXP in the preceding equations represent the bond angle and length values acquired from DFT and experimental calculations. t is the index number of the calculated values of bond angle or bond length, and n denotes the total number of calculated bond angles or lengths. Table 1 contains the error calculation findings from Eqs. (14–17).

The comparison of the experimental and theoretical data to bond angles and lengths reflects a good agreement with slight error deviations in terms of MAD and RMSE, as seen in Table 1. A global comparison was performed by superimposing the molecular skeletons obtained from X–ray diffraction and the theoretical calculations atom by atom, see Fig. 2(b). The obtained RMSE values are 0.3134 Å and 0.0971 Å for B3LYP and ωB97XD levels with 6–311 + + G(*d*,*p*) basis set, respectively. Furthermore, we performed ground state properties calculations using the B3LYP/6-311++G(*d*,*p*) level of theory due to little differences between geometrical properties calculated at B3LYP and ωB97XD levels. The optimized geometries were then used to calculate other parameters, such as electronic and optical properties, absorption spectra, molecular electrostatic potential, and NLO properties.

3.2 Ground state geometry optimization

Ground state geometry optimization was carried out to determine various geometry parameters of the designed compounds since the ground state configuration significantly affects the optoelectronic characteristics of molecular systems. Geometry optimization also affects π—bridging and outlying acceptors on conjugation extension (Marlina et al. 2022a, 2022b). The model bis-chalcones derivatives (**A1** to **A4** and **B1** to **B4**) at their ground state were optimized using the B3LYP method and 6-311++G(*d*,*p*) basis set to reach global minima, i.e., the molecules' lowest probable potential energy.

The specified geometrical parameters, bond lengths (d_1, d_2), and dihedral angles (θ_1, θ_2) optimized using B3LYP/6-311++G (*d*,*p*) methodology are represented in Fig. 3 and listed in Table 2. Figure 4 depicts the optimized structures for the all-new chalcone-core-containing compounds. After optimization, the ideal geometry configurations reveal that the *N*-methyl-4-piperidone bridge retains its planarity throughout

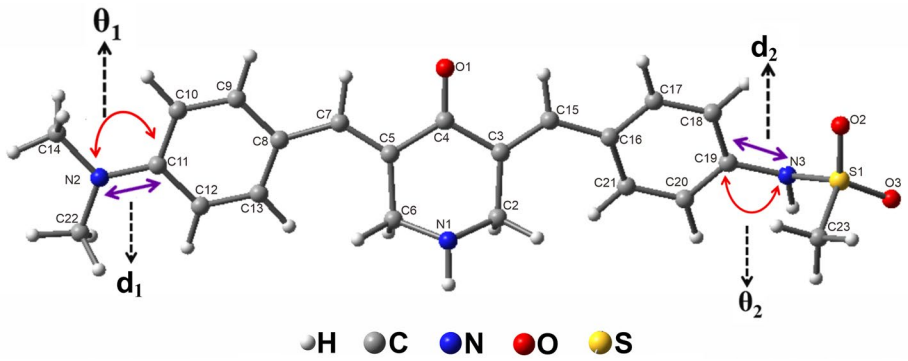

Fig. 3 Schematic representation of bond length and dihedral angle measured from the optimized structures

Table 2 Calculated optimized geometrical parameters of the designed compounds involving bond distance (d_1 and d_2) and dihedral angles (θ_1 and θ_2)

Compounds	Bond lengths (Å)		Dihedral angles (°)	
	d_1	d_2	θ_1	θ_2
A1	1.368	1.425	175.34	− 167.44
A2	1.369	1.415	174.82	143.51
A3	1.368	1.437	175.84	111.58
A4	1.368	1.439	175.44	103.97
B1	1.378	1.424	171.74	− 171.15
B2	1.378	1.416	171.50	143.16
B3	1.376	1.436	172.78	113.85
B4	1.376	1.438	172.59	106.23

all bis-chalcone derivatives. In contrast, curvy geometries are observed in outlying donors or acceptors due to the rotation of these groups in another plane to reduce steric hindrance.

All developed compounds have dihedral angles θ_1 that are close to 180°, especially when utilizing dimethylamine (set **A**). The calculated dihedral angles of the proposed compounds range from 174.82 to 175.84°, showing that the donors and *N*-methyl-4-piperidone bridge are coplanar. This will promote intramolecular charge transport by facilitating electron delocalization. Furthermore, **A4** and **B4** have two values of 103.97° and 106.23°, respectively, which are changed by introducing 2,2,2-trichloroacetamidyl moiety into the molecules. Because of these moieties, **A4** and **B4** have more significant fluctuations in θ_1 value than **A1** to **A3** or **B1** to **B3**. As a result, the twisted conformation of these molecules is caused by the various functional groups present in the acceptor (A). Reduced dihedral angles of **A4** and **B4** promote electron mobility. Furthermore, the distance d_1 values are 1.376–1.369 Å, whereas, for all compounds, the d_2 bond values are nearly equal, in the order of 1.415–1.438 Å. These values are shorter than typical C–C bond lengths (1.530 Å) (Mo et al. 1996), indicating that all molecules have high resonances between the donor and acceptor. The results show that changing the donor and acceptor of **A1** to **A4** and **B1** to **B4** impacts the dihedral angles between the donor, spacer, and acceptor.

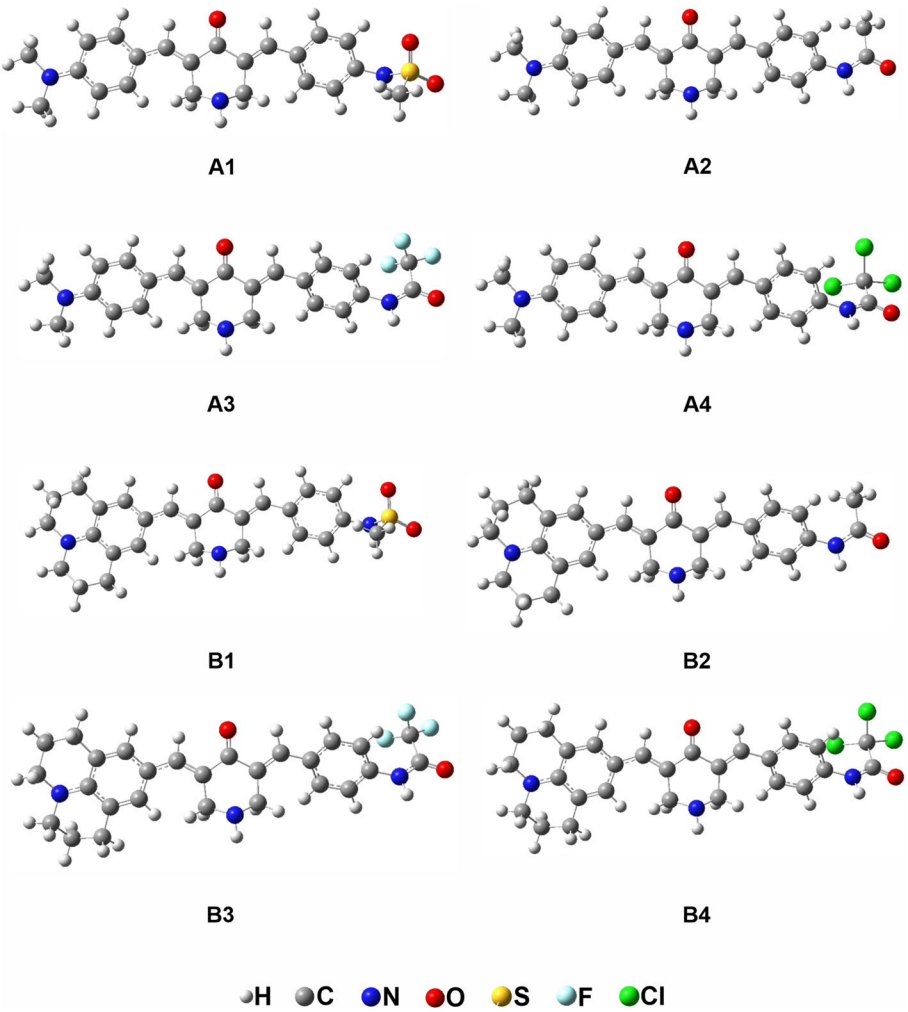

Fig. 4 Optimized geometries of the newly designed compounds. The atomic label numberings of the backbone are referred in Fig. 3

3.3 Ground state electronic structure

3.3.1 Molecular orbital analyses

The electronic structure consists of HOMO and LUMO, with the LUMO preferentially receiving incoming electrons from the HOMO upon electronic excitation (Arunkumar and Anbarasan 2019; Hutama et al. 2019). To achieve the dispersal pattern of electronic density in the HOMO and LUMO, B3LYP/6-311++G(*d,p*) functional was used. The distribution pattern of the electronic cloud derived from the FMO investigations was used to characterize chromophores' electronic and optical responses. The HOMO–LUMO energies' essential roles as electron donors and acceptors explain a chromophore's capacity to absorb light

and reactivity (Hutama et al. 2019). They can also predict the most reactive site in π—electron systems and clarify the types of reactions in resonating systems. The HOMO–LUMO energy gap (Δ_{H-L}) reveals the molecular structure's ability to transfer charges. A small Δ_{H-L} indicates an efficient transfer that boosts the chromophore's NLO activity.

The computed Δ_{H-L} for the investigated compounds in solvent media are presented in Table 3. From the calculated results, the estimated energy gaps for the compounds are in the following order: **B3** < **B4** < **B2** ~ **B1** < **A3** ~ **A4** < **A2** ~ **A1**. **A2** and **B2** are greater than the derivatives at 2.90 eV. This Δ_{H-L} gap is lowered to 2.67 eV in **B3** and **B4** due to the insertion of the D moiety of alkyl amine groups and A moiety of 2,2,2-trifluoroacetamidyl (**B3**) and 2,2,2-trichloroacetamidyl (**B4**) where as a result a strong push–pull architecture (D-π-A) is developed.

Following that, electrons in the compounds drift toward the acceptor side due to the powerful withdrawing capability of the fluoro and chloro groups, which may be responsible for the reduction in their energy gaps: 2.67 eV for **B3** and 2.68 eV for **B4**. Furthermore, a diminishing pattern in the Δ_{H-L} value as 2.86 eV for **A3** and **A4** is noticed. Halogen group substitution, as seen in **A3**, **A4**, **B3**, and **B4** in group **A**, is commonly used to derivatize bis-chalcone derivative geometries. As predicted from **A3**, **A4**, **B3**, and **B4**, inductive electron withdrawal causes the electronic cloud to delocalize further toward the acceptor site at higher substituent electronegativity values. However, the inductive impact and the specific structure of the acceptor molecule may be the reasons for the decrease in the Δ_{H-L} values in both moieties. These chlorinated and fluorinated A species have a stronger ability to pull electrons away from the A unit. This value thus speeds the charge transfer and considerably reduces the energy gap.

FMO computations were used to investigate molecular electronic stability, interactions, reactivity, and optoelectronic characteristics (Gunasekaran et al. 2008).

In general, HOMO can be identified as an electron donor, whereas LUMO is known as an electron acceptor (Amiri et al. 2016). Figure 5 depicts a visual representation of the HOMO and LUMO distributions. The HOMO orbitals of the bis-chalcone derivatives are mainly located around the dimethyl amine aromatic ring and the vinyl double bond. The LUMO, in contrast, is primarily focused on the acceptor moiety and the π—spacer moiety. As a result, an ICT is seen in the designed molecules that connect the D and A parts via a π–bridge. This behavior is precisely like the one observed in the *E* dichloro methoxy chalcones (Yousif and Fadhil 2021). This phenomenon indicates that the intramolecular charge

Table 3 The molecular properties of the designed compounds obtained at the B3LYP/6-311++G(*d*,*p*) level

Molecular properties	A1	A2	A3	A4	B1	B2	B3	B4
E_{HOMO} (eV)	−5.47	−5.47	−5.48	−5.48	−5.25	−5.25	−5.26	−5.26
E_{HOMO} (eV)	−2.57	−2.57	−2.63	−2.63	−2.53	−2.53	−2.59	−2.59
Δ_{H-L} (eV)	2.90	2.90	2.86	2.86	2.73	2.73	2.67	2.68
IP (eV)	5.47	5.47	5.48	5.48	5.25	5.25	5.265	5.26
EA (eV)	2.57	2.57	2.63	2.63	2.53	2.53	2.59	2.59
η (eV)	1.45	1.45	1.43	1.43	1.36	1.36	1.34	1.34
μ (eV)	−4.02	−4.02	−4.06	−4.06	−3.89	−3.89	−3.93	−3.93
S (eV)	0.345	0.345	0.350	0.350	0.367	0.3674	0.374	0.373
ω (eV)	5.56	5.56	5.76	5.76	5.55	5.56	5.77	5.75
μ_{tot} (Debye)	15.77	12.11	14.61	14.05	16.39	13.12	15.57	15.17

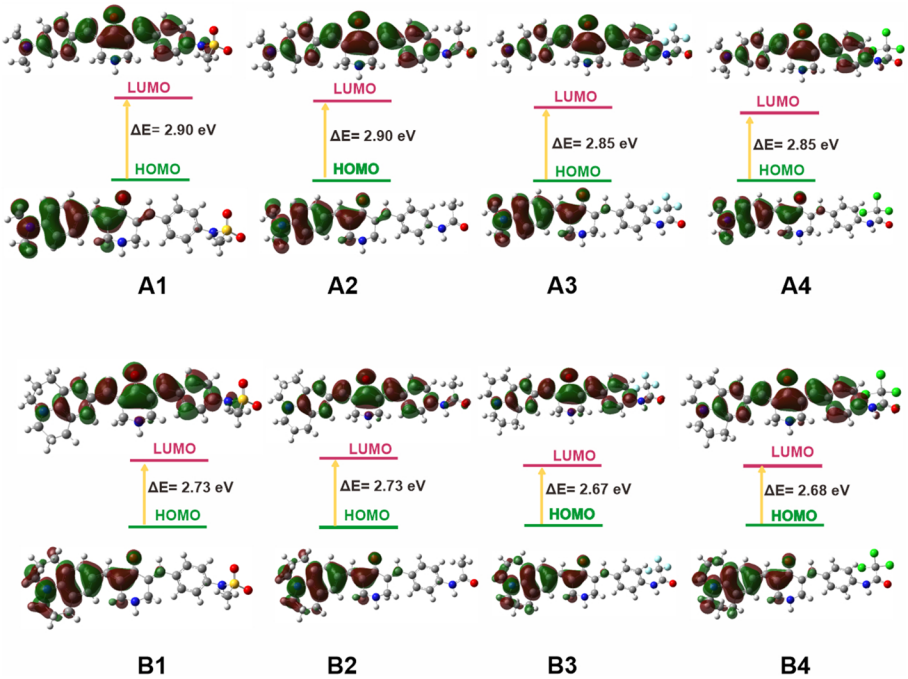

Fig. 5 The HOMO–LUMO representations with their respective orbital energies and orbital energy gaps determined at B3LYP/6–311 + + G(*d*,*p*) level of theory

transfer occurs as a result of the transfer of the electron cloud through the π-conjugated framework from the electron-donor groups, i.e., the dimethyl amine benzene ring, the vinyl double bond, and the carbonyl group, to the electron-acceptor groups.

The location of HOMO and LUMO for the parent molecule (see Supporting Information Fig. S1) do not shift due to the symmetric nature of the parent molecule, while shifting electron density from donor to acceptor region is observed in the LUMO orbitals of the designed compounds, indicating the compounds' potential for successful charge transfer upon excitation. This electronic distribution in HOMO–LUMO allows electron density to be transferred from the donor to the acceptor part of the molecule. In addition, it can be noted that all the compounds suggested are potential NLO materials, as evidenced by this charge transfer.

3.3.2 Chemical reactivity descriptor

HOMO and LUMO energies illustrate the reactivity and stability of the compounds by predicting the CRD derived from the FMO energies (Lesar and Milošev 2009; Parr et al. 1999). The Δ_{H-L} is vital in determining the chemical reactivity and dynamic stability of molecules under investigation. It is well evident from the literature that less reactivity and more stability of any compound are associated with a larger Δ_{H-L}. In contrast, a small HOMO–LUMO energy gap accounts for soft and reactive compounds with less stability (Tahir et al. 2017). The IP and EA derived from the HOMO and LUMO energy values were further used to elucidate various parameters of the CRD, as reported in Table 3.

The EA and IP values are directly related to investigated compounds' electron-accepting and donating character determined from LUMO and HOMO energy, respectively. It is evident from Table 3 that the IP values of compounds **A3** and **A4** are found to be more positive than other compounds, which indicates a more pronounced donating capability. The EA value is positive in all compounds, indicating the possible utilization of these compounds in charge transfer reactions. The EA values are more positive in **A3** and **A4** (2.63 eV) than others, showing their remarkable accepting affinity.

In this investigation, the trend of η for the series of designed bis-chalcone derivatives follows the same trend of the energy gap. Hence, it is worth mentioning that **A1** and **A2**, with the largest Δ_{H-L}, have the highest chemical hardness and, therefore, have the highest thermodynamic stability and smaller reactivity to oxidation and reduction reactions. However, **B4** possesses the lowest energy gap and global hardness and, consequently, is more reactive and softer than the others. These findings can be observed in Table 3 and Eq. (3) since the value S is inversely proportional to the global hardness**.**

The η value of **A1** and **A2** (1.47 eV) is more significant than other studied compounds, describing the more excellent stability and less reactivity of **A1** than the other compounds. On the other hand, the S value is observed to be highest in **B4**, indicating better reactivity and less stability of **B4** than **A1** to **A4** or **B1** to **B3**, holding the lowest softness value, leading to less reactivity and better stability. Overall, findings of global reactivity parameters indicate that energy gap, ionization potential, electronegativity, and hardness values are observed to be greater in **A1**, indicating its better-donating capability, excellent stability, and, at the same time, its less accepting nature and reactivity compared to other studied compounds. On the other hand, electron affinity, electrophilicity, and softness values are greater in **B4**, which suggests that **B4** is a compound with a more accepting nature, highly reactive, less stable, and less donating capability. Therefore, both compounds can play a role in optoelectronic technologies.

3.3.3 Transition density matrix

TDM analysis is essential in determining how acceptor, donor, and π-spacer fragments interact with one another and with the transfer charge. Furthermore, it offers information on the exact positioning of electrons, holes, and electron–hole overlap (Duan et al. 2013). Because hydrogen atoms rarely participate in electron excitation of chemical interest, hydrogen is commonly excluded in the plot to make the map compact. The TDM heat map is a two-dimensional colored display showing the number of atoms along the abscissa (x-axis) and electron density distribution along the y-axis.

Figure 6 depicts the TDM heat maps for all systems. To facilitate the TDM features, all proposed compounds are divided into three parts: donor, π-linker, and acceptor. In TDM analysis, heat maps comprising a band of colors represent the charge transfer from the singlet ground state (S_0) to the first excited state (S_1). In all the designed compounds, the diagonal transition of charge from the electron-donating to the electron-accepting part through the π-spacer is made clear by TDM heat maps. The largest electronic charge density appears at D, considerably at the π-spacer, and very minutely at A, which signifies charge transfer without trapping and enhances the NLO response (Fig. 6). These pictograms also supported the FMO examinations, where the detailed sight of charge transfer is shown.

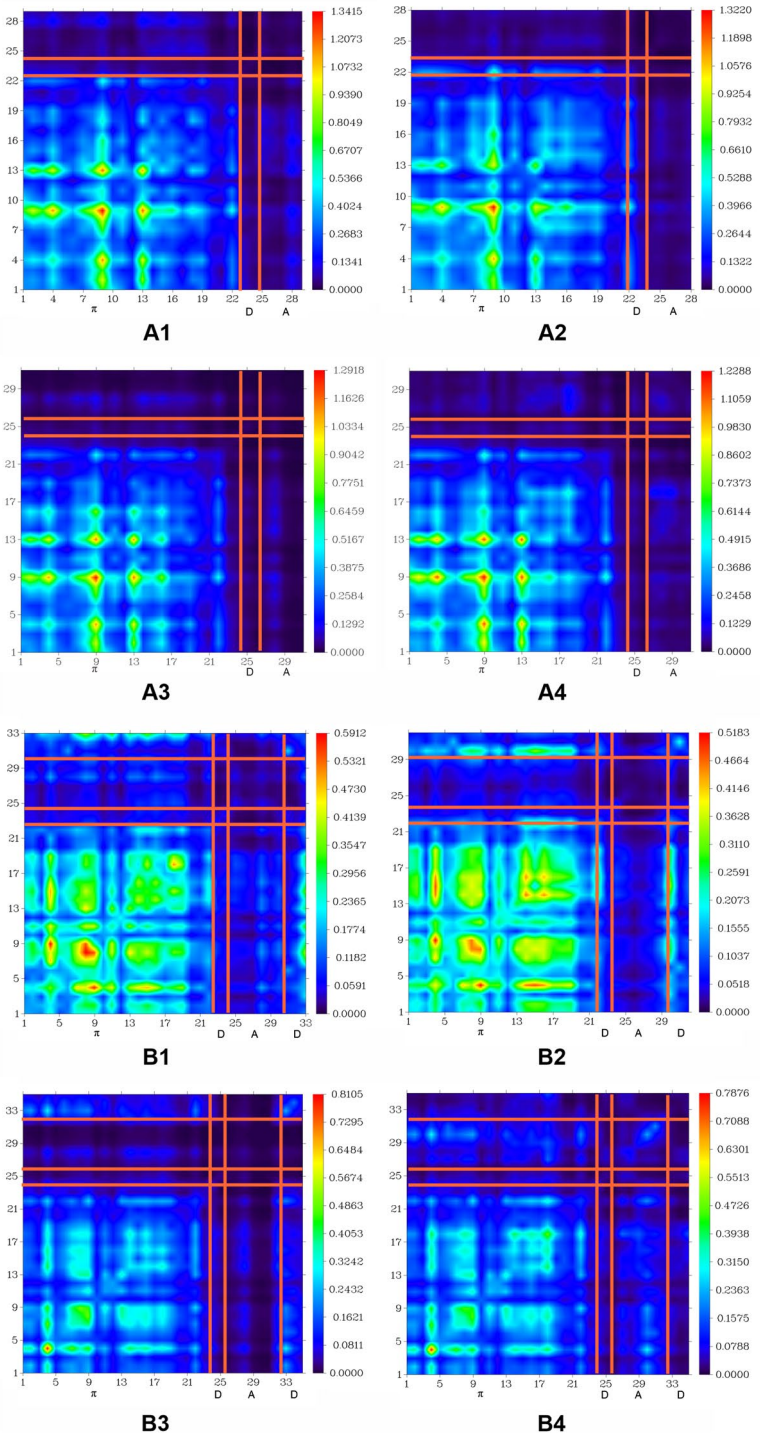

Fig. 6 The transition density matrix heat map for all considered systems

3.3.4 Molecular electrostatic potential

As well known, the MEP diagram helps predict or understand the chemical reactivity behavior of any molecular system. The different colors of the potential represent various electrostatic potential values. Red colors indicate areas with the highest electrostatic potential related to electrophilic attacks. In contrast, blue colors indicate areas with the highest electrostatic potential related to nucleophilic reactivity, such as hydrogen atoms and $–CH_3$ groups. Smaller zones of high potential are shown by yellow and green, which are more significant regions of medium potential (Muhammad et al. 2022, 2017)—the potential increases in the following order: red < orange < yellow < green < blue.

The MEP graphs of the examined compounds are theoretically predicted at the B3LYP/6-311++G(*d*,*p*) level of theory. They are shown in Fig. 7. The nitrogen atoms for the eight bis-chalcone derivatives are in positive regions indicated by blue, denoting a preferred site for nucleophile attack. Meanwhile, the negative regions are primarily localized

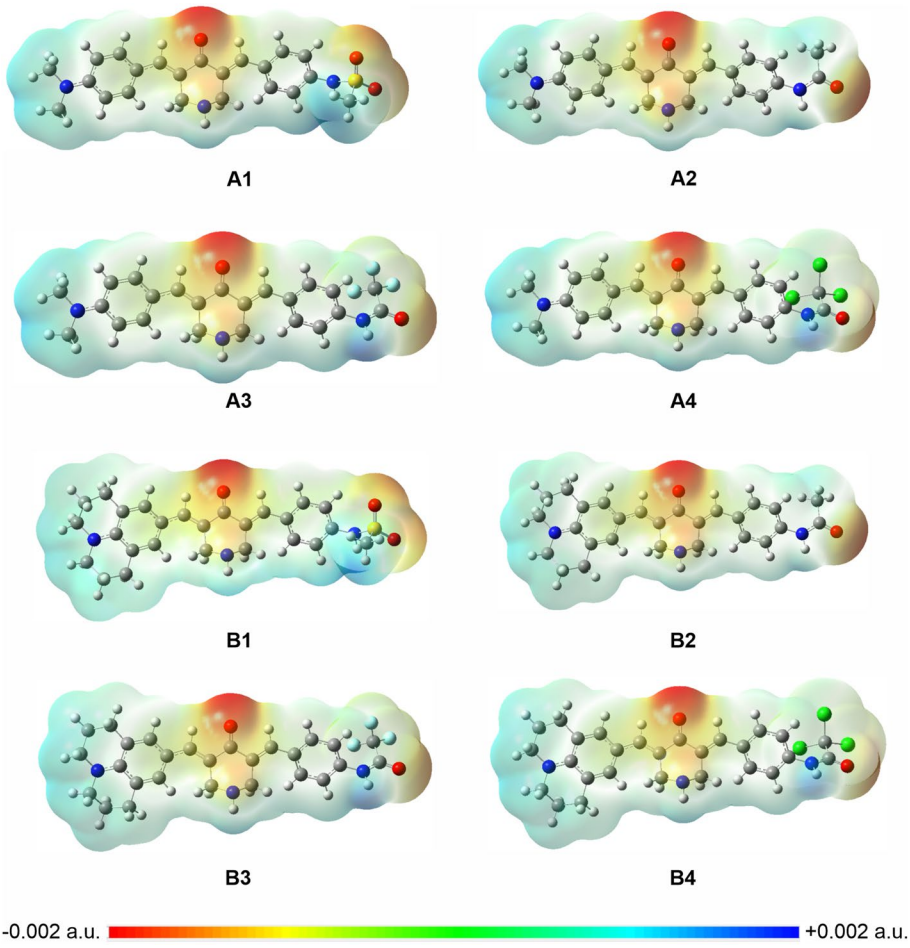

Fig. 7 All systems' molecular electrostatic potential diagram with an isovalue of ± 0.002 a.u. The electrostatic potential decreases from positive to negative as blue > green > yellow > orange > red

on the oxygen atoms of the C=O group, and the orange color indicates electrophilic attack sites—the spread of electron density over the selected compounds results in improved linear and nonlinear optical properties.

3.4 Linear optical properties

Table 4 summarizes all computed transition energies (ΔE), f_0 and other parameters for all studied systems calculated at TD-B3LYP/6-311++G(d,p). The transition states with nearly zero f_0 are considered unfavorable transitions and, therefore, neglected. The most significant transition comes from the $S_1 \leftarrow S_0$ transition. UV–vis spectra are

Table 4 The configuration interaction (CI), electronic excitation type, transition energies (ΔE), oscillator strength (f_o), and transition dipole moment $\Delta\mu$, and the estimated β_{zzz} calculated at TD-B3LYP/6-311 + + G(d,p) level

Compounds	Electronic excitation type	ΔE (eV)	f_0	λ_{max} (nm)	CI	$\Delta\mu$ (Debye)	β_{zzz} (a.u.)
A1	$S_1 \leftarrow S_0$	2.60	1.0785	476.69	HOMO → LUMO (99%)	10.46	7611.18
	$S_4 \leftarrow S_0$	3.46	0.4748	358.18	HOMO-1 → LUMO (55%)	6.01	817.47
A2	$S_1 \leftarrow S_0$	2.60	1.1005	477.40	HOMO-3 → LUMO (98%)	10.57	7886.83
	$S_4 \leftarrow S_0$	3.42	0.3749	363.04	HOMO-1 → LUMO (50%)	5.38	601.24
A3	$S_1 \leftarrow S_0$	2.57	0.9598	482.32	HOMO → LUMO (99%)	9.92	6658.53
	$S_4 \leftarrow S_0$	3.63	0.7277	341.91	HOMO-2 → LUMO (56%)	7.27	1318.05
A4	$S_1 \leftarrow S_0$	2.57	0.9699	482.99	HOMO → LUMO (99%)	9.98	6796.85
	$S_4 \leftarrow S_0$	3.56	0.3656	348.15	HOMO → LUMO + 1 (67%)	5.20	500.07
B1	$S_1 \leftarrow S_0$	2.46	1.0497	504.55	HOMO → LUMO (99%)	10.61	8914.93
	$S_4 \leftarrow S_0$	3.44	0.5482	359.96	HOMO-1 → LUMO (47%)	6.48	1031.86
B2	$S_1 \leftarrow S_0$	2.46	1.0655	504.53	HOMO → LUMO (99%)	10.69	9115.54
	$S_4 \leftarrow S_0$	3.41	0.4616	363.25	HOMO-2 → LUMO (49%)	5.97	823.14
B3	$S_1 \leftarrow S_0$	2.42	0.9468	512.53	HOMO → LUMO (99%)	10.16	8067.16
	$S_4 \leftarrow S_0$	3.51	0.5578	352.97	HOMO → LUMO + 1 (72%)	6.47	988.84
B4	$S_1 \leftarrow S_0$	2.42	0.9593	511.93	HOMO → LUMO (99%)	10.22	8194.35
	$S_6 \leftarrow S_0$	3.61	0.5938	343.33	HOMO-2 → LUMO (47%)	6.58	985.78

essential for getting insights into the linear optical properties of chemical compounds. The calculated UV–Vis spectra for all entitled compounds at TD-B3LYP functional and 6-311++G(*d*,*p*) basis set are provided in Fig. 8. It is seen that the two absorptions λ_{max} for **A1** to **A4** are below 500 nm, which may be ascribed as slight electronic charge redistributions upon electronic transition. The compounds **B3** and **B4** have shown a single absorption wavelength at around 537 nm, where a slight red shift is observable for compounds **B1** and **B2**. Their absorption λ_{max} is seen over a broad range, especially inside visible and near IR spectra regions, as shown in Fig. 8.

The absorption values make it abundantly clear that the presence of the electron-accepting moieties has a major impact on the absorbance shift toward a longer wavelength. In **A1**, it is possible to see the lowest absorbance of 476.69 nm, which corresponds to an oscillation strength of 1.0785 and a transition energy of 2.60 eV. Introducing a strong acceptor unit proves to red-shift the λ_{max} as seen in the compounds **A3**, **A4**, and **B4**. The λ_{max} shifts to 482.32 nm with f_0 of 0.9598 for **A3**, 482.99 nm with f_0 of 0.9699 for **A4**, and 511.93 nm with f_0 of 0.9593 for **B4**. Similar to these results, the λ_{max} for **B3** at 512.53 nm is the longest one, with a transition energy of 2.4191 eV, indicating 99% HOMO → LUMO electronic transitions. Only the first transition will exhibit significant absorption intensity based on oscillator strength and absorption co-efficient values, making the band at 400–500 nm wavelengths the most intense with a HOMO–LUMO contribution of 97–99%. These corresponding transitions might be characterized as the $\pi \rightarrow \pi^*$ transitions for the ICT process from donor fragment to acceptor fragments as exemplified for compound **B3** and **B4** (see inside HOMO–LUMO orbitals in Fig. 5). Besides $\pi \rightarrow \pi^*$ transitions, there are also $n \rightarrow \pi^*$ transitions observed for compounds **A1** to **A4** since $n \rightarrow \pi^*$ transitions involve lower energy, their λ_{max} is longer, about 540 nm for compounds **B1** to **B4**. Due to some symmetry constraints, the absorption intensity of n to π^* transitions is usually lower than $\pi \rightarrow \pi^*$ transitions. This may be the case for molecules **B1** to **B4** at these lower energy and higher wavelength transitions. We found that halogen groups (–F or –Cl) in compounds **A3**, **A4**, **B3**, and **B4** allow additional electronegative atoms to induce an unexpected bathochromic shift in the electronic transitions. Consequently, based on their highest calculated value and narrowest band gap, **A3**, **A4**, **B3**, and **B4** may be considered adequate visible–light absorber molecules.

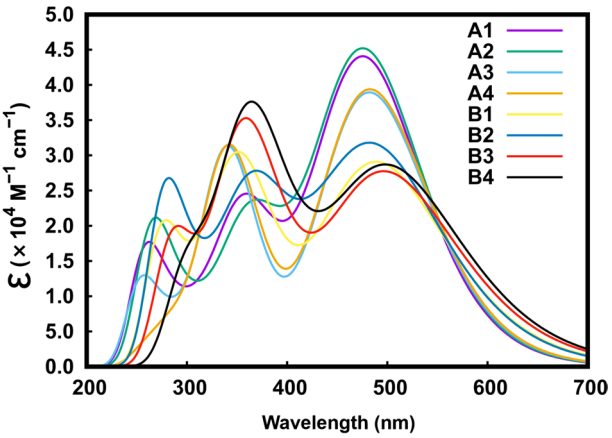

Fig. 8 UV–vis spectra for designed compounds at TD-B3LYP functional and 6–311 + + G(*d*,*p*) basis set. The molar extinction coefficient (ε) is plotted against the absorption wavelength

3.5 Nonlinear optical properties

3.5.1 Estimated hyperpolarizability from a two-level model

Results from the excited-state TD–DFT calculations can also be used to explain the origin of higher-order NLO responses (at least for the dominant diagonal component, β_{zzz}) of several D–π–A molecules based on the conventional two-level models (Andrews et al. 2011; Oudar and Chemla 1976) presented in Eq. (18)

$$\beta_{zzz} = (3/2)\Delta\mu \times \frac{f_o}{\Delta E^3} \tag{18}$$

where ΔE, f_o, $\Delta\mu$ are the transition energy, oscillator strength, and transition dipole moment, respectively. The TD-DFT-estimated β_{zzz} are listed in Table 4. The variation in the dipole moment from the ground state to the excited states ($S_n \leftarrow S_0$) was calculated along the z-axis. These three characteristics are intrinsically connected and are determined by the electronic properties of D–π–A molecules. These models have been widely employed theoretically and experimentally to explain variations in higher-order NLO polarizabilities of diverse D–π–A molecules using spectroscopic characteristics. It can be seen from Eq. (18) that β is directly related to the oscillator strength and transition dipole moment while having an inverse relation with the transition energy. Lower transition energy, higher oscillator strength, and transition moment prove that more charge is transferred, which improves the NLO response.

Excitation energy is considered a critical factor in hyperpolarizability since it is inversely correlated with β_{zzz} in the two-level model, which has been examined in various previously reported excess electron systems (Champagne and Kirtman 2006; Silva et al. 2015). The calculated β_{zzz} values vary from zero to 9115.54×10^{-30} esu, with set **A** showing the lower hyperpolarizability value from the two-level model and set **B** showing the greater value. Due to a significant change in the dipole moment ($\Delta\mu$) and low transition energy, **B2** has the largest β_{zzz} (9115.54×10^{-30} esu). As a result, we can conclude that the shift in dipole moment is the primary determinant of hyperpolarizability β_{zzz} in our examined compounds. The significant value of $\Delta\mu$ causes higher hyperpolarizability (β_{zzz}) values (vide supra). Furthermore, the estimated β_{zzz} values have a strong positive correlation with total hyperpolarizability (β_{tot}). Thus, the validation of a two-level model provides substantial insight into their NLO response, where evidence to study the nonlinearity of researched compounds can be found.

3.5.2 Static nonlinear optical properties from ground-state calculations

The charge transfer occurs from extended-conjugated systems of organic compounds' electron-donating and electron-accepting characteristics (Marlina et al. 2022a, 2022b). First, the static α_{tot} and β_{tot} values of derivative compounds were determined using various DFT functionals, including B3LYP, CAM–B3LYP, M06, and ωB97XD, to understand the effect of different DFT functionals. The comparative hyperpolarizability results of B3LYP, CAM-B3LYP, M06 and ωB97XD DFT functional reveal the highest β_{tot} value of various derivative compounds is observed for B3LYP, followed by CAM–B3LYP, ωB97XD and M06. Although the β_{tot} of **A1** and **A2** are smaller ($< 200 \times 10^{-30}$ esu), the NLO response of the bis-chalcone derivative is relatively bigger for hybrid functionals than the long-range

Table 5 Static first hyperpolarizability (β_{tot}) of designed compounds for different DFT functionals calculated with 6-311++G(*d*,*p*) basis set. The polarizability (α_{tot}) and the vectorial part of the first hyperpolarizability (β_{vec}) were calculated at B3LYP/6-311++G(*d*,*p*) level of theory

Compounds	β_{tot} ($\times 10^{-30}$ esu)				α_{tot} ($\times 10^{-24}$ esu)	β_{vec} ($\times 10^{-30}$ esu)
	ωB97XD	B3LYP	CAM-B3LYP	M06		
A1	161.73	348.37	182.79	266.59	85.61	312.05
A2	167.05	336.89	189.07	275.58	84.15	332.83
A3	206.67	420.67	234.24	347.54	81.64	397.03
A4	205.31	418.98	231.75	344.13	89.61	402.41
B1	236.36	470.34	270.90	405.43	97.08	424.22
B2	224.32	464.46	256.13	378.95	95.53	457.20
B3	268.60	558.11	307.48	464.64	93.38	525.48
B4	262.85	554.11	299.67	451.09	101.15	532.80

corrected DFT functionals. The results listed in Table 5 show that the fraction of Hartree–Fock (HF) exchange in the DFT functional contributes to the magnitude of NLO parameters within the DFT functional. Smaller β_{tot} values have been obtained for compound **A1** (Table 5 and Fig. 9) using long-range corrected functionals CAM–B3LYP and ωB97XD which contain larger amounts of HF exchange, whereas the B3LYP level gives the highest β_{tot} values.

For example, the most significant NLO response of the reported complexes with B3LYP and M06 functionals could be attributed to the highest contribution of the HF exchange in B3LYP and M06 hybrid functionals, which are above 25% (Wykes et al. 2013) and 27% (Walker et al. 2013), respectively. With ωB97XD, the HF exchange for short-range is reduced to 22%, lowering the hyperpolarizability values concerning the HF exchange contribution (Thomas et al. 2016). The β_{tot} of the proposed compounds is further reduced for CAM–B3LYP, most likely due to a reduction in HF exchange to 19% for short-range and 65% for long-range (Shao et al. 2020; Yanai et al. 2004). As also seen in Table S1, the larger basis set shows no remarkable effects on the NLO properties. Therefore, we chose the 6-311++G(*d*,*p*) basis set for this section because of the good balance between the accuracy of the results and the reasonable computational cost. Overall, these novel bischalcone derivatives have hyperpolarizabilities that are noticeably high at the B3LYP/6-311++G(*d*,*p*) level of theory; hence, complete descriptions of these approaches are

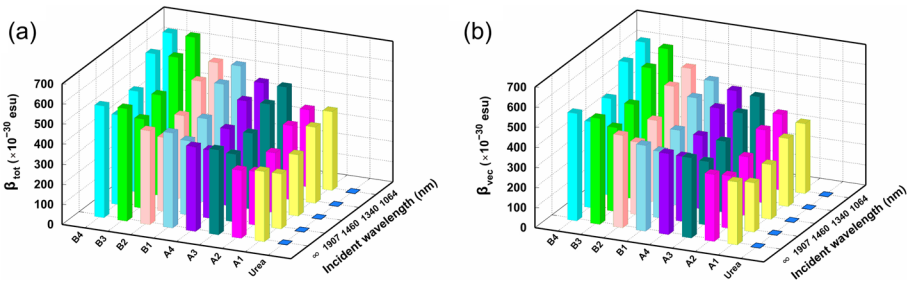

Fig. 9 Calculated static (β_∞) and dynamic first hyperpolarizabilities of the compounds at B3LYP/6–311 + + G(*d*,*p*) level of theory: **a** the total hyperpolarizability (β_∞) and **b** the vectorial part of β_{tot} (β_{vec})

provided below. For these reasons, NLO properties of different derivatives were evaluated using the DFT method at B3LYP/6-311++G(*d*,*p*) level. Many DFT levels, especially B3LYP functional in combination with the 6-311++G(*d*,*p*) basis set, are commonly and effectively employed to calculate NLO characteristics of molecular systems (Chen et al. 2022; Tamer et al. 2014). Although B3LYP is a versatile and widely used functional for many types of electronic structure calculations, it may have limitations for predicting the NLO properties accurately. NLO properties are method-dependent, where B3LYP may struggle to capture these dependencies accurately, mainly when dealing with large or flexible molecules (Morgante and Peverati 2020). In any case, a recent theoretical study (Hutama et al. 2019) shows that B3LYP shows sufficient accuracy in predicting the β_{tot} values for the halogen-substituted *N*-methyl-4-piperidone curcumin analog compounds.

The μ_{tot}, which can be orientated arbitrarily in a molecular frame, determines the NLO properties. The magnitude of the anticipated NLO coefficients is determined by the μ_{tot}, which is more prominent in the excited state than in the ground state surrounding influencing media such as solvents (Oudar and Chemla 2008). According to the literature, the urea molecule is employed as a standard molecule for the relative examination of dipole moment and initial hyperpolarizability values (Adant et al. 1995). All the compounds have dipole moments greater than urea's (5.49 Debye). The overall μ_{tot} values observed are as follows: **A2** < **A4** < **A3** < **A1** for set **A** and **B2** < **B4** < **B3** < **B1** for set **B** (see Table 3), which suggests that **A2** possesses the lowest dipole moment among the molecules.

Similarly, the increasing order of average linear polarizability of the designed compounds is as follows: **A3** < **A2** < **A4** < **A1** for set **A** and **B3** < **B2** < **B1** < **B4** for set **B**. Because the **A2** molecule has a dipolar form, the contribution of free partial charges is minimal. The molecules of **A1** and **B1** with sulfonamide-substituted contribute a remarkably high amount of partial charges compared to the molecule of **A2**. Due to sulfur and halogen groups (–F o r–Cl), which have inductively positive effects, **A1**, **A3**, **A4**, **B1**, **B3** and **B4** are more polar than **A2** and **B2**. Because of its good donating ability, it can be deduced that the alkyl amine-substituted in *para*-position of the B set molecules represents the most significant net dipole moment among all molecules from **A1** to **A4** or **B1** to **B4** (Tu et al. 2023).

As shown in Table S2, the polarizability tensor along the *z*axis is more dominating in all compounds, and its contribution to linear polarizability is more significant than others. The analysis of this table reveals that no component of the static dipole polarizability and the first hyperpolarizability has a negligible value. Based on the calculated static α_{tot} and anisotropic polarizability ($\Delta\alpha$), the biggest α_{tot} and $\Delta\alpha$ are found in **B4**, with $\alpha_{tot} = 101.15 \times 10^{-24}$ esu and $\Delta\alpha = 110.36 \times 10^{-24}$ esu. That molecule has static average isotropic and total anisotropic polarizability values of 16.37 and 41.68 times, respectively, larger than urea (Abbas et al. 2019). Including three halogen groups, which enriched the electronic structure surrounding the A unit and increased the electron-withdrawing ability, was linked to a notable increase in its value. The degree to which substituents were added to the halogenated acetamidyl unit acceptor (**A3**, **A4**, **B3**, and **B4**) altered a molecule's nonlinearity. The conjugated system's contribution increases and becomes more dominant when replacements occur.

In the case of the β_{tot}, the dominant contribution to β_{tot} is made by the *z*-axis direction transition with positive values. According to Marlina et al. (2022b) the energy gap between LUMO and HOMO influences the polarizability of the molecule. Molecules with small energy gaps and high linear polarizability values typically exhibit more significant hyperpolarizability values. This statement is true for the system that we investigated. For example, the decreasing order of β_{tot} values **B4** > **B3** > **B1** > **B2** is found to be following the linear trend with the polarizability where the highest α_{tot} is achieved in molecule **B4**, which

reverse to the energy gap order **B4** ~ **B3** < **B1** ~ **B2**. Thus, the β_{tot} value of B set was found to be relatively lower in the case of **B2** (464.46×10^{-30} esu) compared to **B3** (558.11×10^{-30} esu). Due to the addition of a fluoro (−F) group, which improves the accepting tendency of molecules from the opposing ends, **A3** and **B3** exhibit better NLO responses than the other proposed compounds. The –F group effectively improves the NLO dimensions for **A3** and **B3** because it is more electron withdrawing than the –Cl or –S groups. This is because a fluorine atom in acceptor moieties provides a significantly higher amplitude of intramolecular interaction energy, resulting in a significant rise in strain energy. Furthermore, in the case of **A3**, **A4**, **B3,** and **B4**, there is an alkylamine as a donor component in addition to the three halogen atoms on the acceptor that compete from opposing ends. The highest and lowest NLO responses in these compounds can also be examined via π-linked interactions inside each donor–acceptor scheme tested. A higher degree of electron delocalization results in a smaller HOMO–LUMO energy differential and increased hyperpolarizability (β_{tot}) values in the proposed compounds.

3.5.3 Frequency-dependent polarizability and hyperpolarizability

Combining static and dynamic calculations offers a holistic view of molecules' NLO properties. Static calculations provide information about the ground-state properties, while dynamic calculations reveal how they respond to time-varying fields (Prommin et al. 2019). This comprehensive understanding is valuable for predicting the molecule's behavior in various experimental conditions. The responses of the tensor components of dynamic hyperpolarizabilities at the molecular level can be used to understand how a molecule reacts to an applied external electric field (Hutama et al. 2019). The *x*, *y*, and *z* polarizability tensor components were used to calculate the dynamic polarizability $\alpha(\omega;\omega)$ at different frequencies (or wavelengths), where the employed ω were 0.02389, 0.03121, 0.03400, and 0.04282 a.u—corresponding to the incident wavelength of 1907, 1460, 1340, and 1064 nm, respectively. The employed wavelengths are the most common laser wavelengths employed in experiments.

Table S2 shows that the components β_z are the ones that contribute the most to the average values of dynamics polarizability and first-order hyperpolarizability in molecules at different frequencies. According to the calculations, the best values in couples **A1** to **A4** and **B1** to **B4** were achieved with molecules **A3**, **A4**, **B3**, and **B4**, with **A4** and **B4** having the highest value at all frequencies (see Fig. 9a). For example, at the highest frequency of 0.04282 a.u. (1064 nm), the β_{tot} values of **A3**, **A4**, **B3** and **B4** are 1,682.04, 1,625.07, 2,222.57 and 2,223.96 times greater than that of urea (0.28×10^{-30} esu). According to this study, the first-order hyperpolarizability of bis-chalcone derivatives is much higher than that of reference urea material. It may be stated that charge distribution in these molecules is easily distorted when an external electric field is applied, resulting in good NLO capabilities for use in optoelectronics and optical systems. Notably, the obtained values of dynamic isotropic and anisotropic polarizability at the frequency of 0.04282 a.u. are higher than those of static polarizability values. Furthermore, based on the obtained data, we discover that the polarizability of the molecule is closely related to the variation of incident frequencies. For example, the dynamic first hyperpolarizability β (-ω;ω,ω) of molecule **A4** at $\beta_{(\lambda=1907\ nm)}$, $\beta_{(\lambda=1460\ nm)}$, $\beta_{(\lambda=1340\ nm)}$, and $\beta_{(\lambda=1064\ nm)}$ is 443.50×10^{-30}, 499.56×10^{-30}, 622.7×10^{-30} and 661.22×10^{-30} esu, respectively (see Table S2). It becomes clear that as the applied frequency increases, so does the dynamic first hyperpolarizability.

To support these findings, the projection of static hyperpolarizability onto the dipole moment vector (β_{vec}) was also computed (see Fig. 9b). The trend of β_{vec} is precisely consistent with the β_{tot} of the designed compounds, revealing that **A3**, **A4**, **B3**, and **B4** molecules are highly NLO sensitive while **B1** and **B2** systems show minor sensitivity. These findings are comparable to the above-mentioned electronic parameters, especially the HOMO–LUMO gap and CRD analysis.

Overall, the results show that all of the compounds studied are polarizable. The shift of electronic density from donor to acceptor group in molecules plays a significant role in improving β. When the appropriate electron-withdrawing and electron-donating groups are attached at the opposing terminal of the main skeleton, the electron push–pull mechanism operates efficiently, and electronic movement occurs, resulting in a sizeable β value. The comparison with the urea study shows that all studied compounds are suitable NLO candidates. **A3**, **A4**, **B3**, and **B4** have overcome the challenge with maximum linear polarizability and hyperpolarizability. According to the findings, the nature and side of substitution of different groups (donor or acceptor) on the conjugated chain significantly influence the NLO properties of proposed derivative compounds. Indeed, based on our findings, the resonance effects in designed molecules may be the driving force behind the ICT (Hrobarik et al. 2010), and these compounds might be promising candidates for developing NLO devices and technology-related applications.

4 Conclusion

The present work aims to study the arrangement of donor–acceptor groups on linear and NLO response properties of the computational study of bis-chalcone derivatives. Halogenated-acetamide acts as the electron acceptor group of molecules **A3**, **A4**, **B3,** and **B4** and consists of dimethylaniline as the electron donor. Ground state DFT and TD–DFT have been employed to optimize the geometry of the molecules, followed by computation of total dipole moment, static and dynamic first hyperpolarizability. The results reveal that the dipole moment and total static first hyperpolarizability (β_{tot}) of the studied molecules are dominated by the respective components in the direction of charge transfer. The ratio of the vector component of the first hyperpolarizability to β_{tot} (β_{vec}) also supports the unidirectional charge transfer in the studied systems. In molecules **A3**, **A4**, **B3** and **B4**, which are donor–bridge–acceptor (D–π–A)-type systems, the halogen-acetamide acceptor moiety is found to play a significant role in controlling the NLO response over the other acceptor groups. The results presented are expected to pave the way to tuning the NLO response of many ICT-based bis-chalcone derivatives, especially those with D–π–A arrangements. To summarize the data, better results have been obtained for designed bis-chalcone derivatives compared to urea. It can be concluded that the designed organic compounds would be promising materials in the field of NLO.

Supplementary Information The online version contains supplementary material available at https://doi.org/10.1007/s11082-023-05383-7.

Acknowledgements LAM acknowledges postdoctoral funding from the Manajemen Talenta BRIN fellowship program 2023 No. 15/II/HK/2023. The calculations were partly performed at Mahameru High-Performance Computing, National Research and Innovation Agency (BRIN) and SymBaHCat Cluster belonging to the Symbah Foundation.

Authors' contribution LAM conceived the idea, led the investigation and methodology, and equally contributed to data curation, formal analysis, funding acquisition, and writing the original draft. ASH contributed

equally to formal analysis, supervision, validation, and original draft writing. SNZ and MFP provided support in the investigation. WJS assisted in writing, reviewing, and editing the manuscript. WDS took the lead in supervision and equally contributed to reviewing and editing the manuscript.

Funding L.A.M. acknowledges funding from Manajemen Talenta BRIN fellowship program 2023 No. 15/II/HK/2023.

Availability of data and materials The datasets generated during and/or analyzed during the current study are available from the corresponding author on reasonable request.

Declarations

Competing interests The authors declare no competing interests.

Ethical approval Not applicable.

References

Abbas, H., Shkir, M., AlFaify, S.: Density functional study of spectroscopy, electronic structure, linear and nonlinear optical properties of l-proline lithium chloride and l-proline lithium bromide monohydrate: for laser applications. Arab. J. Chem. **12**, 2336–2346 (2019). https://doi.org/10.1016/j.arabjc.2015.02.011

Adant, C., Dupuis, M., Bredas, J.L.: Ab initio study of the nonlinear optical properties of urea: electron correlation and dispersion effects. Int. J. Quantum Chem. **56**, 497–507 (1995). https://doi.org/10.1002/qua.560560853

Amiri, S.S., Makarem, S., Ahmar, H., Ashenagar, S.: Theoretical studies and spectroscopic characterization of novel 4-methyl-5-((5-phenyl-1, 3, 4-oxadiazol-2-yl) thio) benzene-1, 2-diol. J. Mol. Struct. **1119**, 18–24 (2016)

Ammasi, A., Iruthayaraj, R., Munusamy, A.P., Shkir, M.: Molecular engineering on D–π–A organic dyes with flavone-based different acceptors for highly efficient dye-sensitized solar cells using experimental and computational study. J. Mol. Model. **29**, 45 (2023a). https://doi.org/10.1007/s00894-023-05445-3

Ammasi, A., Iruthayaraj, R., Munusamy, A.P., Shkir, M., Vellingiri, B., Minnam Reddy, V.R., Kim, W.K.: Molecular screening of different π-linker-based organic dyes for optoelectronic applications: quantum chemical study. J. Electron. Mater. **52**, 3774–3785 (2023b). https://doi.org/10.1007/s11664-023-10338-5

Andrews, D.L., Bradshaw, D.S., Coles, M.M.: Perturbation theory and the two-level approximation: a corollary and critique. Chem. Phys. Lett. **503**, 153–156 (2011). https://doi.org/10.1016/j.cplett.2010.12.055

Arunkumar, A., Anbarasan, P.M.: Optoelectronic properties of a simple metal-free organic sensitizer with different spacer groups: quantum chemical assessments. J. Electron. Mater. **48**, 1522–1530 (2019). https://doi.org/10.1007/s11664-018-06912-x

Barone, V., Cossi, M.: Quantum calculation of molecular energies and energy gradients in solution by a conductor solvent model. J. Phys. Chem. A **102**, 1995–2001 (1998). https://doi.org/10.1021/jp9716997

Becke, A.D.: Density-functional thermochemistry. III. The role of exact exchange. J. Chem. Phys. **98**, 5648–5652 (1993). https://doi.org/10.1063/1.464913

Bernstein, J., Davis, R.E., Shimoni, L., Chang, N.-L.: Patterns in hydrogen bonding: functionality and graph set analysis in crystals. Angew. Chem. Int. Ed. EngL. **34**, 1555–1573 (1995). https://doi.org/10.1002/anie.199515551

Bosshard, C., Hulliger, J., Florsheimer, M., Gunter, P.: Organic Nonlinear Optical Materials. CRC Press, Boca Raton (2001)

Cai, Z.-B., Bai, L., Pan, Y.-L., Ma, F.-F., Li, S.-L., Tian, Y.-P.: Multipolar symmetric and asymmetric N–heterocyclic compounds with efficient two−photon absorption. J. Photochem. Photobiol. A Chem. **346**, 194–205 (2017)

Chai, J.-D., Head-Gordon, M.: Long-range corrected hybrid density functionals with damped atom–atom dispersion corrections. Phys. Chem. Chem. Phys. **10**, 6615–6620 (2008)

Champagne, B., Kirtman, B.: Evaluation of alternative sum-over-states expressions for the first hyperpolarizability of push-pull π-conjugated systems. J. Chem. Phys. (2006). https://doi.org/10.1063/1.2206181

Chattaraj, P.K., Maiti, B., Sarkar, U.: Philicity: a unified treatment of chemical reactivity and selectivity. J. Phys. Chem. A **107**, 4973–4975 (2003)

Chen, R., Xu, K., Wang, G., Zhang, Z., Cao, L., Teng, B.: Theoretical and experimental investigation of a pyridinium-based NLO crystal 4-N, N-dimethylamino-4′-N′-methyl-stilbazolium 3,4-dimethoxy-sulfonate. Optik (stuttg). **257**, 168830 (2022). https://doi.org/10.1016/j.ijleo.2022.168830

Chidan Kumar, C.S., Quah, C.K., Balachandran, V., Fun, H.-K., Asiri, A.M., Chandraju, S., Karabacak, M.: Synthesis, single crystal structure, spectroscopic characterization and molecular properties of (2E)-3-(2,6-dichlorophenyl)-1-(3,4-dimethoxyphenyl)prop-2-en-1-one. J. Mol. Struct. **1116**, 135–145 (2016). https://doi.org/10.1016/j.molstruc.2016.02.089

Christodoulides, D.N., Khoo, I.C., Salamo, G.J., Stegeman, G.I., Van Stryland, E.W.: Nonlinear refraction and absorption: mechanisms and magnitudes. Adv. Opt. Photonics. **2**, 60–200 (2010)

Cigan, M., Donovalová, J., Szöcs, V., Gaspar, J., Jakusová, K., Gaplovsky, A.: 7-(Dimethylamino) coumarin-3-carbaldehyde and its phenylsemicarbazone: TICT excited state modulation, fluorescent H-aggregates, and preferential solvation. J. Phys. Chem. A **117**, 4870–4883 (2013)

Cisse, L., Djande, A., Capo-Chichi, M., Delatre, F., Saba, A., Tine, A., Aaron, J.-J.: Revisiting the photophysical properties and excited singlet-state dipole moments of several coumarin derivatives. Spectrochim. Acta. Part A Mol. Biomol. Spectrosc. **79**, 428–436 (2011)

Cossi, M., Rega, N., Scalmani, G., Barone, V.: Energies, structures, and electronic properties of molecules in solution with the C-PCM solvation model. J. Comput. Chem. **24**, 669–681 (2003). https://doi.org/10.1002/jcc.10189

Duan, Y., Geng, Y., Li, H., Jin, J., Wu, Y., Su, Z.: Theoretical characterization and design of small molecule donor material containing naphthodithiophene central unit for efficient organic solar cells. J. Comput. Chem. **34**, 1611–1619 (2013)

Erickson, M.A., Beels, M.T., Biaggio, I.: Optimum conjugation length in donor–acceptor molecules for third-order nonlinear optics. JOSA B **33**, E130–E142 (2016)

Eryanti, Y., Herlina, T., Zamri, A., Shiono, Y., Awang, K., Halim, S.N.A., Supratman, U.: N-benzyl-(3E,5E)-3,5-bis(2-hydroxybenzylidene)-4-piperidone. Molbank **2015**, 5–8 (2015). https://doi.org/10.3390/M852

Fejer, M.M.: Nonlinear optical frequency conversion. Phys. Today **47**, 25–33 (1994)

Feng, L., Maddox, M.M., Alam, M.Z., Tsutsumi, L.S., Narula, G., Bruhn, D.F., Wu, X., Sandhaus, S., Lee, R.B., Simmons, C.J.: Synthesis, structure–activity relationship studies, and antibacterial evaluation of 4-chromanones and chalcones, as well as olympicin A and derivatives. J. Med. Chem. **57**, 8398–8420 (2014)

Frisch, M.J., Trucks, G.W., Schlegel, H.B., Scuseria, G.E., Robb, M.A., Cheeseman, J.R., Scalmani, G., Barone, V., Mennucci, B., Petersson, G.A., Nakatsuji, H., Caricato, M., Li, X., Hratchian, H.P., Izmaylov, A.F., Bloino, J., Zheng, G., Sonnenberg, J.L., Hada, M., Ehara, M., Toyota, K., Fukuda, R., Hasegawa, J., Ishida, M., Nakajima, T., Honda, Y., Kitao, O., Nakai, H., Vreven, T., Montgomery, J.A., Jr., Peralta, J.E., Ogliaro, F., Bearpark, M., Heyd, J.J., Brothers, E., Kudin, K.N., Staroverov, V.N., Kobayashi, R., Normand, J., Raghavachari, K., Rendell, A., Burant, J.C., Iyengar, S.S., Tomasi, J., Cossi, M., Rega, N., Millam, J.M., Klene, M., Knox, J.E., Cross, J.B., Bakken, V., Adamo, C., Jaramillo, J., Gomperts, R., Stratmann, R.E., Yazyev, O., Austin, A.J., Cammi, R., Pomelli, C., Ochterski, J.W., Martin, R.L., Morokuma, K., Zakrzewski, V.G., Voth, G.A., Salvador, P., Dannenberg, J.J., Dapprich, S., Daniels, A.D., Farkas, Ö., Foresman, J.B., Ortiz, J.V., Cioslowski, J., Fox, D.J.: Gaussian-09 Revision D.01. Gaussian, Inc., Wallingford (2013)

Gandhimathi, R., Vinitha, G., Dhanasekaran, R.: Effect of substituent position on the properties of chalcone isomer single crystals. J. Cryst. Process Technol. **3**, 148–155 (2013)

Garmire, E.: Nonlinear optics in daily life. Opt. Express. **21**, 30532–30544 (2013)

Ghouili, A., Dusek, M., Petricek, V., Ayed, T.B., Hassen, R.B.: Synthesis, crystal structure and spectral characteristics of highly fluorescent chalcone-based coumarin in solution and in polymer matrix. J. Phys. Chem. Solids. **75**, 188–193 (2014). https://doi.org/10.1016/j.jpcs.2013.09.011

Gunasekaran, S., Balaji, R.A., Kumeresan, S., Anand, G., Srinivasan, S.: Experimental and theoretical investigations of spectroscopic properties of N-acetyl-5-methoxytryptamine. Can. J. Anal. Sci. Spectrosc. **53**, 149–162 (2008)

Hagar, M., Ahmed, H.A., Aljohani, G., Alhaddad, O.A.: Investigation of some antiviral N-heterocycles as COVID 19 drug: molecular docking and DFT calculations. Int. J. Mol. Sci. **21,** 3922 (2020). https://doi.org/10.3390/ijms21113922

Hrobarik, P., Sigmundova, I., Zahradnik, P., Kasak, P., Arion, V., Franz, E., Clays, K.: Molecular engineering of benzothiazolium salts with large quadratic hyperpolarizabilities: can auxiliary electron-withdrawing groups enhance nonlinear optical responses? J. Phys. Chem. C **114**, 22289–22302 (2010)

Hussein, H.A., Fadhil, G.F.: Theoretical Investigation of para amino-dichloro chalcone isomers. Part II: a DFT structure-stability study of the FMO and NLO properties. ACS Omega **8**, 4937–4953 (2023). https://doi.org/10.1021/acsomega.2c07148

Hutama, A.S., Huang, H., Kurniawan, Y.S.: Investigation of the chemical and optical properties of halogen-substituted N-methyl-4-piperidone curcumin analogs by density functional theory calculations. Spectrochim. Acta Part A Mol. Biomol. Spectrosc. **221**, 117152 (2019). https://doi.org/10.1016/j.saa.2019.117152

Irfan, A., Al-Sehemi, A.G., Assiri, M.A., Mumtaz, M.W.: Exploring the electronic, optical and charge transfer properties of acene-based organic semiconductor materials. Bull. Mater. Sci. **42**, 1–7 (2019a)

Irfan, A., Chaudhry, A.R., Al-Sehemi, A.G., Assiri, M.A., Hussain, A.: Charge carrier and optoelectronic properties of phenylimidazo [1, 5-a] pyridine-containing small molecules at molecular and solid-state bulk scales. Comput. Mater. Sci. **170**, 109179 (2019b)

Ito, M., Mikami, N.: Multiphoton spectroscopy. Appl. Spectrosc. Rev. **16**, 299–352 (1980)

Ivanova, B.B., Spiteller, M.: Noncentrosymmetric crystals with marked nonlinear optical properties. J. Phys. Chem. A **114**, 5099–5103 (2010)

Kuebler, S.M., Rumi, M.: NONLINEAR OPTICS, APPLICATIONS | Three-Dimensional Microfabrication. In: Encyclopedia of Modern Optics. pp. 189–206. Elsevier (2005)

Kusumawati, Y., Ivansyah, A.L., Ali, B.T.I., Kurnia, K.A., Hutama, A.S., Fansuri, H.: Photophysical properties of ammonium, pyrrolidinium, piperidinium, imidazolium, and pyridinium as a guide to prepare ionic-organic hybrid materials. Heliyon **8**, e09121 (2022). https://doi.org/10.1016/j.heliyon.2022.e09121

Lee, C., Yang, W., Parr, R.G.: Development of the Colle-Salvetti correlation-energy formula into a functional of the electron density. Phys. Rev. B **37**, 785–789 (1988). https://doi.org/10.1103/PhysRevB.37.785

Lesar, A., Milošev, I.: Density functional study of the corrosion inhibition properties of 1, 2, 4-triazole and its amino derivatives. Chem. Phys. Lett. **483**, 198–203 (2009)

Lifshitz, R., Arie, A., Bahabad, A.: Photonic quasicrystals for nonlinear optical frequency conversion. Phys. Rev. Lett. **95**, 133901 (2005)

Lu, T., Chen, F.: Multiwfn: a multifunctional wavefunction analyzer. J. Comput. Chem. **33**, 580–592 (2012). https://doi.org/10.1002/jcc.22885

Maidur, S.R., Patil, P.S., Ekbote, A., Chia, T.S., Quah, C.K.: Molecular structure, second-and third-order nonlinear optical properties and DFT studies of a novel non-centrosymmetric chalcone derivative:(2E)-3-(4-fluorophenyl)-1-(4-{[(1E)-(4-fluorophenyl) methylene] amino} phenyl) prop-2-en-1-one. Spectrochim. Acta Part A Mol. Biomol. Spectrosc. **184**, 342–354 (2017)

Majumder, M., Misra, A.: Strategic design of thiophene-fused nickel dithiolene derivatives for efficient NLO response. Phys. Chem. Chem. Phys. **20**, 19007–19016 (2018)

Marlina, L.A., Haryadi, W., Daengngern, R., Pranowo, H.D.: Molecular design of benzo[c][1,2,5]thiadiazole or thieno[3,4-d]pyridazine-based auxiliary acceptors through different anchoring groups in D–π–A–A framework: a DFT/TD-DFT study. J. Mol. Graph. Model. **113**, 108148 (2022a). https://doi.org/10.1016/j.jmgm.2022.108148

Marlina, L.A., Haryadi, W., Pranowo, H.D.: Design of a D–π–A–A framework with various auxiliary acceptors on optoelectronic and charge transfer properties for efficient dyes in DSSCs: a DFT/TD-DFT study. J. Comput. Electron. **21**, 361–377 (2022b). https://doi.org/10.1007/s10825-022-01851-7

Mary, Y.S., Panicker, C.Y., Anto, P.L., Sapnakumari, M., Narayana, B., Sarojini, B.K.: Molecular structure, FT-IR, NBO, HOMO and LUMO, MEP and first order hyperpolarizability of (2E)-1-(2, 4-Dichlorophenyl)-3-(3, 4, 5-trimethoxyphenyl) prop-2-en-1-one by HF and density functional methods. Spectrochim. Acta Part A Mol. Biomol. Spectrosc. **135**, 81–92 (2015)

Matos, M.J., Vazquez-Rodriguez, S., Uriarte, E., Santana, L.: Potential pharmacological uses of chalcones: a patent review (from June 2011–2014). Expert Opin. Ther. Pat. **25**, 351–366 (2015)

Miar, M., Shiroudi, A., Pourshamsian, K., Oliaey, A.R., Hatamjafari, F.: Theoretical investigations on the HOMO–LUMO gap and global reactivity descriptor studies, natural bond orbital, and nucleus-independent chemical shifts analyses of 3-phenylbenzo [d] thiazole-2 (3 H)-imine and its para-substituted derivatives: Solvent and substituent effects. J. Chem. Res. **45**, 147–158 (2021)

Mo, Y., Lin, Z., Wu, W., Zhang, Q.: Bond-distorted orbitals and effects of hybridization and resonance on C–C bond lengths. J. Phys. Chem. **100**, 11569–11572 (1996). https://doi.org/10.1021/jp953433a

Morgante, P., Peverati, R.: The devil in the details: a tutorial review on some undervalued aspects of density functional theory calculations. Int. J. Quantum Chem. **120**, e26332 (2020). https://doi.org/10.1002/qua.26332

Muhammad, S.: Symmetric vs. asymmetric: Which one is the better molecular configuration for achieving robust NLO response? J. Mol. Graph. Model. **114**, 108209 (2022). https://doi.org/10.1016/j.jmgm.2022.108209

Muhammad, S., Al-Sehemi, A.G., Su, Z., Xu, H., Irfan, A., Chaudhry, A.R.: First principles study for the key electronic, optical and nonlinear optical properties of novel donor-acceptor chalcones. J. Mol. Graph. Model. **72**, 58–69 (2017)

Muhammad, S., Nakano, M., Al-Sehemi, A.G., Irfan, A., Chaudhry, A.R., Tonami, T., Ito, S., Kishi, R., Kitagawa, Y.: Exploring the novel donor-nanotube archetype as an efficient third-order nonlinear optical material: asymmetric open-shell carbon nanotubes. Nanoscale **10**, 16499–16507 (2018)

Muhammad, S., Sarwar, F., Bibi, S., Nadeem, R., Mushtaq, M.W., Al-Sehemi, A.G., Alarfaji, S.S., Hussain, S.: Insighting the functionally modified C60 fullerenes as an efficient nonlinear optical materials: aA quantum chemical study. Mater. Sci. Semicond. Process. **141**, 106421 (2022)

Naik, V.S., Patil, P.S., Wong, Q.A., Quah, C.K., Gummagol, N.B., Jayanna, H.S.: Molecular structure, linear optical, second and third-order nonlinear optical properties of two non-centrosymmetric thiophene-chalcone derivatives. J. Mol. Struct. **1222**, 128901 (2020)

Nakano, M., Fukuda, K., Champagne, B.: Third-order nonlinear optical properties of asymmetric nonalternant open-shell condensed-ring hydrocarbons: effects of diradical character, asymmetricity, and exchange interaction. J. Phys. Chem. C **120**, 1193–1207 (2016)

Nesterov, V.N.: 3,5-Bis(4-methoxybenzylidene)-1-methyl-4-piperidone and 3,5-bis(4-methoxybenzylidene)-1-methyl-4-oxopiperidinium chloride: Potential biophotonic materials. Acta. Crystallogr. Sect. C Cryst. Struct. Commun. **60**, 806–809 (2004). https://doi.org/10.1107/S0108270104022723

Oudar, J.L., Chemla, D.S.: Hyperpolarizabilities of the nitroanilines and their relations to the excited state dipole moment. J. Chem. Phys. **66**, 2664–2668 (1976). https://doi.org/10.1063/1.434213

Oudar, J.L., Chemla, D.S.: Hyperpolarizabilities of the nitroanilines and their relations to the excited state dipole moment. J. Chem. Phys. **66**, 2664–2668 (2008). https://doi.org/10.1063/1.434213

Panicker, C.Y., Varghese, H.T., Nayak, P.S., Narayana, B., Sarojini, B.K., Fun, H.K., War, J.A., Srivastava, S.K., Van Alsenoy, C.: Infrared spectrum, NBO, HOMO–LUMO, MEP and molecular docking studies (2E)-3-(3-nitrophenyl)-1-[4-piperidin-1-yl]prop-2-en-1-one. Spectrochim. Acta Part A Mol. Biomol. Spectrosc. **148**, 18–28 (2015). https://doi.org/10.1016/j.saa.2015.03.065

Parr, R.G., Szentpály, L.V., Liu, S.: Electrophilicity index. J. Am. Chem. Soc. **121**, 1922–1924 (1999)

Ponnusamy Munusamy, A., Ammasi, A., Shkir, M.: Computational analysis of carbazole-based newly efficient D–π–A organic spacer dye derivatives for dye-sensitized solar cells. Struct. Chem. **33**, 1097–1107 (2022). https://doi.org/10.1007/s11224-021-01853-4

Prasad, P.N., Williams, D.J.: Introduction to Nonlinear Optical Effects in Molecules and Polymers. Wiley, New York (1991)

Prommin, C., Kerdpol, K., Saelee, T., Kungwan, N.: Effects of π-expansion, an additional hydroxyl group, and substitution on the excited state single and double proton transfer of 2-hydroxybenzaldehyde and its relative compounds: TD-DFT static and dynamic study. New J. Chem. **43**, 19107–19119 (2019). https://doi.org/10.1039/c9nj05055h

Shao, Y., Mei, Y., Sundholm, D., Kaila, V.R.I.: Benchmarking the performance of time-dependent density functional theory methods on biochromophores. J. Chem. Theory Comput. **16**, 587–600 (2020). https://doi.org/10.1021/acs.jctc.9b00823

Silva, D.L., Fonseca, R.D., Vivas, M.G., Ishow, E., Canuto, S., Mendonca, C.R., De Boni, L.: Experimental and theoretical investigation of the first-order hyperpolarizability of a class of triarylamine derivatives. J. Chem. Phys. **142**, 064312 (2015). https://doi.org/10.1063/1.4906893

Sumithra, I.S., Jayashri, T.A., Krishnan, G.: X-ray diffraction, spectroscopic, thermal and surface morphological studies of gamma-irradiated diaquamalonatomanganese(II) (DMM). J. Radioanal. Nucl. Chem. **307**, 835–842 (2016). https://doi.org/10.1007/s10967-015-4283-2

Sutradhar, T., Misra, A.: Theoretical study on the nonlinear optical property of boron nitride nanoclusters functionalized by electron donating and electron accepting groups. J. Phys. Chem. A. **125**, 2436–2445 (2021)

Tahir, M.N., Khalid, M., Islam, A., Mashhadi, S.M.A., Braga, A.A.C.: Facile synthesis, single crystal analysis, and computational studies of sulfanilamide derivatives. J. Mol. Struct. **1127**, 766–776 (2017)

Tamer, Ö., Avci, D., Atalay, Y.: Calculations of electronic structure and nonlinear optical parameters of 4-methoxybenzaldehyde-N-methyl-4-stilbazolium tosylate*. J. Appl. Spectrosc. **80**, 971–982 (2014). https://doi.org/10.1007/s10812-014-9875-z

Tejkiran, P.J., Teja, M.S.B., Kumar, P.S.S., Sankar, P., Philip, R., Naveen, S., Lokanath, N.K., Rao, G.N.: DA–π–D Synthetic approach for thienyl chalcones–NLO–a structure activity study. J. Photochem. Photobiol. A Chem. **324**, 33–39 (2016)

Thamarai, A., Vadamalar, R., Raja, M., Muthu, S., Narayana, B., Ramesh, P., Muhamed, R.R., Sevvanthi, S., Aayisha, S.: Molecular structure interpretation, spectroscopic (FT-IR, FT-Raman), electronic solvation (UV–Vis, HOMO-LUMO and NLO) properties and biological evaluation of (2E)-3-(biphenyl-4-yl)-1-(4-bromophenyl) prop-2-en-1-one: experimental and computational modeling. Spectrochim. Acta Part A Mol. Biomol. Spectrosc. **226**, 117609 (2020)

Thomas, A., Chitumalla, R.K., Puyad, A.L., Mohan, K.V., Jang, J.: Computational studies of hole/electron transport in positional isomers of linear oligo-thienoacenes: evaluation of internal reorganization energies using density functional theory. Comput. Theor. Chem. **1089**, 59–67 (2016)

Tu, Y., Chai, K., Wu, J., Hu, Y., Shi, S., Yang, D., Yao, T.: A rational design to improve selective imaging of tau aggregates by constructing side substitution on N, N-dimethylaniline/quinoxaline D–π–A fluorescent probe. Sens. Actuators B Chem. **380**, 133406 (2023). https://doi.org/10.1016/j.snb.2023.133406

Vazquez-Rodriguez, S., López, R.L., Matos, M.J., Armesto-Quintas, G., Serra, S., Uriarte, E., Santana, L., Borges, F., Crego, A.M., Santos, Y.: Design, synthesis and antibacterial study of new potent and selective coumarin–chalcone derivatives for the treatment of tenacibaculosis. Bioorg. Med. Chem. **23**, 7045–7052 (2015)

Virkki, M., Tuominen, O., Forni, A., Saccone, M., Metrangolo, P., Resnati, G., Kauranen, M., Priimagi, A.: Halogen bonding enhances nonlinear optical response in poled supramolecular polymers. J. Mater. Chem. C **3**, 3003–3006 (2015)

Walker, M., Harvey, A.J.A., Sen, A., Dessent, C.E.H.: Performance of M06, M06–2X, and M06-HF density functionals for conformationally flexible anionic clusters: M06 functionals perform better than B3LYP for a model system with dispersion and ionic hydrogen-bonding interactions. J. Phys. Chem. A **117**, 12590–12600 (2013)

Wazzan, N., Irfan, A.: Exploring the optoelectronic and charge transport properties of pechmann dyes as efficient OLED materials. Optik (stuttg) **197**, 163200 (2019)

Wei, H., Ruan, J., Zhang, X.: Coumarin–chalcone hybrids: promising agents with diverse pharmacological properties. RSC Adv. **6**, 10846–10860 (2016)

Wykes, M., Milián-Medina, B., Gierschner, J.: Computational engineering of low bandgap copolymers. Front. Chem. **1**, 35 (2013)

Yanai, T., Tew, D.P., Handy, N.C.: A new hybrid exchange-correlation functional using the Coulomb-attenuating method (CAM-B3LYP). Chem. Phys. Lett. **393**, 51–57 (2004). https://doi.org/10.1016/j.cplett.2004.06.011

Yoneda, K., Nakano, M., Fukuda, K., Matsui, H., Takamuku, S., Hirosaki, Y., Kubo, T., Kamada, K., Champagne, B.: Third-order nonlinear optical properties of one-dimensional open-shell molecular aggregates composed of phenalenyl radicals. Chem. Eur. J. **20**, 11129–11136 (2014)

Yousif, A.A., Fadhil, G.F.: DFT of para methoxy dichlorochalcone isomers. Investigation of structure, conformation, FMO, charge, and NLO properties. Chem. Data Collect. **31**, 100618 (2021)

Yushina, I.D., Masunov, A.E., Lopez, D., Dyakov, A.A., Bartashevich, E.: V: Toward first-principles design of organic nonlinear optical materials: Crystal structure prediction and halogen bonding impact on hyperpolarizabilities of 2-iodo-3-hydroxypyridine. Cryst. Growth Des. **18**, 5069–5079 (2018)

Zhao, Y., Truhlar, D.G.: Density functionals with broad applicability in chemistry. Acc. Chem. Res. **41**, 157–167 (2008). https://doi.org/10.1021/ar700111a

Zyss, J.: Molecular Nonlinear Optics: Materials, Physics, and Devices. Academic Press, Cambridge (2013)

Authors and Affiliations

Lala Adetia Marlina[1] · Aulia Sukma Hutama[2] · Septiana Nur Zanah[2] · Mokhammad Fajar Pradipta[2] · Wilin Julian Sari[1] · Wahyu Dita Saputri[1]

✉ Aulia Sukma Hutama
aulia.sukma.hutama@ugm.ac.id

✉ Wahyu Dita Saputri
wahyu.dita.saputri@brin.go.id

Lala Adetia Marlina
lala002@brin.go.id

Septiana Nur Zanah
septiananur99@mail.ugm.ac.id

Mokhammad Fajar Pradipta
fajar@ugm.ac.id

Wilin Julian Sari
wilin.julian.sari@brin.go.id

[1] Research Center for Quantum Physics, National Research and Innovation Agency (BRIN), South Tangerang 15314, Indonesia

[2] Department of Chemistry, Faculty of Mathematics and Natural Sciences, Universitas Gadjah Mada, Yogyakarta 55281, Indonesia